New craniodental remains of carnivorous marsupials from the late Miocene Alcoota Local Fauna of the Northern Territory, Australia. Part 1. *Thylacinus potens* (Dasyuromorphia: Thylacinidae).

New craniodental specimens that are referrable to the thylacinid marsupial, *Thylacinus potens,* are described from the late Miocene Alcoota Local Fauna of the Northern Territory, Australia. The remains include a largely complete maxilla and dentary, showing for the first time the anterior dentition of the dentary. The new remains indicate that *Th. potens* was a more variable species than previously recognised. The dentary, in particular, is more gracile, than other specimens referred to this species. A revised apomorphy-based diagnosis of *Th. potens* that takes this variability into account is presented. A cladisitic analysis supports previous analyses that placed *Th. potens* in a derived position within Thylacinidae, close to the modern *Th. cynocephalus*. New estimations of body size are made using published regressions of dental measurements of dasyuromorphians as well as by assuming geometric similitude with *Th. cynocephalus*. All methods produce body mass estimates in excess of 35 kg.

1 Adam M. Yates

2 Museums and Art Galleries of the Northern Territory

3 Museum of Central Australia, P.O. Box 831, Alice Springs, Northern Territory, 0871

4 Australia

5 Corresponding author: Adam M. Yates, Museum of Central Australia, P.O. Box 831, Alice

6 Springs, Northern Territory, 0871, Australia, ph. +61 (08) 89511148, email:

7 adamm.yates@nt.gov.au

Introduction

The Alcoota Local Fauna is known from a dense bone bed in the lower part of the Waite Formation, cropping out on Alcoota Station, 110 km NE of Alice Springs in south central Northern Territory (Woodburne, 1967). The Waite Formation is a late Cenozoic sequence of fluviatile silts, sands and minor limestone beds filling the Waite Basin, a small intermontane basin, surrounded by crystalline rocks of the Arunta Block (Woodburne, 1967). The bone bed covers an area of approximately 25000 m^2, although its density and thickness varies considerably within that area (Megirian, 2000). The bonebed usually lies 90 cm below the present soil surface, underneath a reddish, weathered horizon (Murray & Megirian, 1992). The bulk of the known fossil material has been obtained from three pits: Paine Quarry, South Pit and Main Pit. Paine Quarry was excavated by Woodburne and colleagues from 1962 to 1963. It was presumably backfilled at the end of Woodburne's field investigations in 1963. South Pit and Main Pit were opened by a team from MAGNT in the mid 1980's and have been kept open and have been more or less continually excavated up to the present. The precise location of Paine Quarry in relation to the MAGNT pits has always been uncertain but recent work matching old, long-lived trees to those present in Woodburne's original field photographs indicates that it lay immediately west of the present day South Pit (Fig. 1).

Based on stage-of-evolution correlation it is thought that the fauna is late Miocene in age (Stirton, Woodburne & Plane, 1967; Murray & Megirian, 1992), and lies somewhere between 5 and 12 million years old (Megirian et al., 2010). The fauna is dominated by large browsing herbivores, both mammalian and avian. Mammalian carnivores are exceptionally rare and restricted to just three known species: *Thylacinus potens*, *Tyarrpecinus rothi* and *Wakaleo alcootaensis* (Woodburne, 1967; Murray & Megirian, 2000; Archer & Rich, 1982). Of these, *Ty. rothi* is a small thylacinid, weighing about 5 kg (Wroe, 2001) that is known only from a single fragmentary specimen (Murray & Megirian, 2000). In contrast *Th. potens* is among the largest of all thylacinids, possibly reaching a bodyweight close to 40kg (Wroe, 2001). Its original hypodigm consisted of a palatal fragment of a skull which was designated the holotype, two jaw fragments, some teeth and a few postcranial elements from the hind foot, all from Paine Quarry (Woodburne, 1967). Only a few postcranial elements, a canine crown, a largely uninformative molar fragment and a single heavily worn and broken molar from Main Pit have been added to this collection over the years between 1963 and 2013.

During the 2013 field season a new pit was opened between the Main Pit and South Pit, at the same stratigraphic height as these two quarries (Fig. 1). This new pit, named 'Shattered Dreams', proved to be exceptionally densely packed with fragmented bones, interspersed with occasional complete, or near complete specimens. Not only was the volume of fossil bone extraordinarily high but the diversity was also high with almost all of the known taxa from the Alcoota Local Fauna recovered from an excavated area of less than two square meters. Among these specimens are postcranial elements as well as upper and lower jaw bones bearing teeth that are referrable to *Th. potens*. In addition an isolated premolar was discovered in South Pit. These are the first

substantial craniodental remains of this species to be recovered since Woodburne's initial excavation of the Alcoota local fauna, 50 years previously.

These new specimens expand our knowledge of the anatomy of ~~this species~~ and its range of variation. As a result of this new information the diagnosis of the species is revised. With more complete specimens at hand, new estimates of the size of *Th. potens* are also calculated.

Methods

Terminology

Cheek teeth are numbered topologically and do not necessarily imply serial homology with other mammals. Thus the three premolars are numbered 1-3, from anterior to posterior and the four molars are numbered 1-4, anterior to posterior.

Institutional Abbreviations are as follows: CPC, Commonwealth Palaeontological Collection, Bureau of Mineral Resources, Canberra; NTM, Museum and Art Gallery of the Northern Territory, Darwin and Alice Springs; SAM, South Australian Museum, Adelaide; UCMP, Museum of Paleontology, University of California, Berkeley.

Size Estimation

Two methods were used to calculate the body size of the new *Th. potens* specimens: NTM P4326 and NTM P4327. Firstly, some of Myers' (2001) regressions were selected. These regressions were derived to predict bodymass of marsupials from a series of craniodental measurements. Three such regressions were used, all derived from the restricted dasyuromorphian dataset. The regression for lower molar tooth row was used to estimate the mass of the dentary specimen (NTM P4327) while the regressions for upper molar tooth row length and width of M^2 was used for the maxilla specimen (NTM P4326). Unfortunately M^1 of NTM P4326 is badly damaged and isolated from the rest of the molar row. Consequently the length of the upper molar tooth row could only be estimated, hence the use of the second, less accurate predictive variable.

The second method used to estimate body mass follows that of Wroe (2001), who assumed geometric similitude between large-bodied species of *Thylacinus* and obtained a scaling factor by comparing measurements of the fossils with the average of the same measurement from *Th. cynocephalus*. In this study the measurements used to obtain the scaling factors were lower molar tooth row length for the dentary specimen (NTM P4327) and the combined length of M^{2-4} for the maxilla specimen (NTM P4326). Average values for *Th. cynocephalus* were obtained from Wroe (2001, table 4) and Woodburne (1967, table 1). An average mass of 29.5 kg for *Th. cynocephalus* (Paddle 2000) was used to scale body mass.

Cladistic Analysis

Several cladistic analyses of thylacinid and dasyuromorphian phylogeny have been attempted. However, no published character-taxon matrix includes all available informative characters and all thylacinid taxa described to date. Therefore a new matrix was assembled by combining data

from previous analyses with the addition of some new character scores for *Th. potens* and *Th. megiriani*. The ingroup was restricted to Thylacinidae and characters that were uninformative within the restricted ingroup were excluded. New character states for *Th. potens* were taken from the specimens describing in this article while new character states for *Th. megiriani* were taken from undescribed lower jaw specimens held in the NTM collections (NTM P4376, 4377). Terminal taxa used and their sources of character data are given in Table 1. Characters (Appendix 1) were taken from Murray (1997), Muirhead & Wroe (1998), Wroe & Musser (2001), Murray & Megirian (2006) with some modification. A few novel characters were added.

The resulting matrix was subjected to a maximum parsimony analysis in PAUP 4.0b (Swofford, 2001) using the following settings: heuristic search; random addition sequence with 500 replicates; and TBR branch-swapping algorithm. The strength of the internal nodes was tested with a bootstrap analysis (1000 bootstrap replicates, heuristic searching with 50 addition sequence replicates).

Systematic Palaeontology

Dasyuromorphia Gill, 1872

Thylacinidae Bonaparte, 1838

Thylacinus potens Woodburne, 1967

New material. NTM P4326, right maxilla in 2 parts, with complete P^{2-3}, M^{2-4}, and fragments of P^1 and M^1 from Shattered Dreams (Figs. 2-8); NTM P4332, isolated left P^3 from South Pit (Fig. 9); NTM P4379, maxillary fragment with broken and worn right M^2 from Main Pit (Fig. 10); NTM P4327, left dentary with P_{2-3}, M_{1-4} and root fragments of P_1 from Shattered Dreams (Fig. 11-14); NTM P4461, crown of right C_1 from Main Pit (Fig. 15); NTM P4516, fragment of right upper molar, possibly M^1, from an unrecorded site of the Alcoota Local Fauna.

Emended diagnosis. Thylacinid distinguished by the following unambiguous autapomorphies: long axis of P^1 mesiobuccally oriented in adults; mesial width of the first upper molar greater than its mesial-distal length; reduced palatal fenestrae approximately one third the length of the upper molar tooth row; absence of a diastema between P_1 and P_2; P_2 longer than P_3 and M_1. The following ambiguous synapomorphies serve to distinguish *Th. potens* from *Th. cynocephalus* (and most fossil thylacinids): ventrally facing sulcus forming the ventral border of the root of the zygomatic arch on the maxilla; P^2 longer than M^1.

Description

Maxilla

The maxilla (NTM P4326) includes the tall side wall of the rostrum that is absent in the holotype. The height of the maxilla above the anterior edge of P^3 is 44.4 mm which is 67.3% of the distance from the mesial margin of the canine to the distal margin of P^3 or approximately 42% of the total

length of the cheek tooth row. These proportions lie with the range of *Th. cynocephalus* (Table 2). Furthermore, the anterodorsal margin of the maxilla rises from the level of the canine to the level of P^3 at an angle of 32° (Fig. 3A), which matches the angle seen in *Th. cynocephalus*. These observations indicate that the snout of *Th. potens* was probably not proportionately shorter or deeper than that of *Th. cynocephalus* and that the crowding of the premolar teeth seen in this species is more likely to be the result of relative enlargement of these teeth as opposed to relative shortening of the jaw. In anterior view the lateral wall of the maxilla slopes dorsomedially, indicating that the rostrum was triangular in cross section.

Ventrally the palatal shelf of the maxilla is complete between the canine and P^2. It indicates that the anterior palate in this region was flat and narrow and was located just a couple of millimetres above the lingual alveolar margins. Doubling the distance from the lingual side of the posterior root of P^1 to the midline symphysis indicates that the total width of the palate between the posterior roots of P^1 is 19.2 mm, distance almost identical to that of the holotype specimen. This is unusually narrow in comparison to *Th. cynocephalus*, and lies at the small end of the range displayed by that species (Table 2), indicating that *Th. potens* may have had a relatively narrow anterior end of the snout (Fig. 2C). A small notch at the anterior end of the preserved portion of the palate is the posterior end of the incisive foramen. It indicates that in this specimen the posterior terminations of these foramina lay between the anterior ends of the canine alveoli, well anterior their position in *Th. cynocephalus* where they terminate between the canine and P1. The palate behind the incisive foramen is simple and flat without the depression or low transverse ridge seen in the holotype.

The posterior maxillary fragment bears the ventral floor of the infraorbital canal on its dorsal surface (Fig 6C, 7C). From the extent of the broken medial and lateral walls of this canal it is apparent that the lateral opening of this canal, the infraorbital foramen, lay above M^2 (Fig. 5B), approximately level with its midlength, as it does in *Th. cynocephalus*. The lateral margin of the canal dwindles anteriorly to a thin ridge that terminates posterior to the contact between M^1 and M^2, indicating that the infraorbital foramen could not have occupied the anterior position that it does in the holotype of *Th. potens*. As in the holotype there is a well-developed, ventrally-facing sulcus incised into the posterior lateral surface of the maxilla, forming the ventral margin of the anterior root of the zygomatic arch (6A, D, 7A, D). Also resembling the holotype is a well-developed pit on the palate between the protocone alveoli of M^3 and M^4. There is a much shallower and less distinct fossa in the analogous position between M^2 and M^3. Two short sections of natural edge are present along the largely broken medial margin of the maxillary shelf level with M^1 and M^2. These represent part of the lateral margin of the palatal vacuity. They indicate that the vacuity lay just 5.8 mm from the protocone of M^2, however there is not enough edge preserved to determine the relative size of the vacuity. Neither is the maxillary shelf complete enough to determine the posterior width of the palate.

Maxillary dentition

The canine alveolus indicates a large, buccolingually compressed and anteriorly directed canine. As in the holotype, the premolars are significantly larger than those of *Th. cynocephalus* (Table

3). The double-rooted P^1 is represented by its alveolus and the posterior root bearing a small remnant of the crown. Although none of the crown morphology can be determined it is apparent from the alveolus that the long axis of the tooth in occlusal view is canted buccomesially relative to the long axis of the canine and the succeeding premolars (Fig 3B, 4B). The out-turned mesial margin of the P^1 alveolus lies buccal to the distal margin of the canine alveolus. In lateral view the two margins draw level with each other so that there is no diastema between the two teeth.

A short diastema of 3.0 mm separates P^1 from P^2. P^2, like the other premolars, is a mesiodistally elongate and buccolingually compressed, double-rooted tooth. It is worn to such a degree that the crown is reduced to a low, bluntly rounded, mound-like structure with no discernable cusps. The long axis of the crown in occlusal view is aligned with that of P^3. The tooth is distinctly wider at its distal end that at its mesial end. Although the crowns of P^2 and P^3 do not contact each other their respective alveoli are in contact and there is no diastema between them (Fig. 3B, 4B).

P^3 is also heavily worn although the large central protocone remains discernable and distinct from the distal heel of the crown. NTM P4332 is an isolated P^3 in a less worn state (Fig. 9). It shows that the protocone formed a tall conical spike with its apex directed slightly distally. The protocone has a rounded cross-section with no cristae extending up either the mesial or distal sides. The mesial face of the protocone forms a surface that continues to the base of the crown without any change in slope or development of anterior bulges or cuspules. There is a suggestion of a basal bulge on the mesial side of the P^3 of NTM P4326 but this is an artefact produced by a wear facet on the mesial face of the protocone. The mesioventrally sloping mesial profile continues in a straight line onto the upper part of the root before curving distally, creating a distinctly rounded profile in lateral view. The distal profile of the crown has a distinct basal heel, separated from the distal margin of the protocone by an inflection. A second rounded distal cuspule arises from the distalolingual surface of the crown base. This cuspule is positioned basal to the level of the distal heel. The distal root extends straight down and is not curved like the mesial root. Due to the breakage of NTM P4332 it is not possible to determine if there was a diastema between P^3 and M^1.

A fragment of M^1 was recovered from the gap between the two maxillary fragments of NTM P4326. It includes the protocone and the buccomesial corner of the tooth and their respective roots. The protocone is set lower than the paracone and stylar cusp B, as it is in the other molars. It is worn flat in mesial view and is rounded in occlusal view. A weakly developed precingulum extends along the mesial margin from the linguomesial corner of the protocone to stylar cusp B. A distinct flexus in the middle of the mesial margin divides the precingulum into two parts, one bordering the protocone, the other the paracone/stylar cusp B complex. The paracone is a low, rounded tubercle. The lingual side of the paracone is somewhat 'tented' with a rounded ridge sloping down from the apex of the paracone to the valley that divides it from the protocone. The precingulum terminates in a poorly developed stylar cusp B. This cusp is no more than a low rounded bulge situated on the buccomesial side of the paracone.

M^2 is complete although somewhat worn. In occlusal view there is a shallow ectoflexus between stylar cusps B and D, at about 40 % of the length of the buccal margin from the mesial end (Fig.

8), unlike the holotype which bears a deep ectoflexus similar to that of M^3. The mesial and linguodistal margins bear weakly developed constrictions in occlusal view, between the protocone and the buccal cusps. A narrow, rudimentary precingulum slopes basally from the mesial side of stylar cusp B to a point near the base of the mesial side of the crown, below the paracone. The low talon is broadly U-shaped in occlusal view and bears a slightly raised protocone on its lingual apex. The preprotocrista, if it was ever present, has been obliterated by a large steeply angled wear facet occupying the mesial face of the talon. The weakly developed postprotocrista extends horizontally along the linguodistal margin of the talon, terminating immediately lingual to the minute metaconule. The metaconule forms a barely-raised, narrow, semi-lunate shelf around the lingual base of the metacone. The paracone has been worn flat, though its smaller base indicates that it was almost certainly subordinate to the metacone before wear. No paracristae remain but the premetacrista component of the centrocrista can be seen extending down the mesial side of the metacone to the worn base of the paracone. The metacone is the largest cusp of the tooth, its apex has been worn off forming an oblique buccodistally facing wear facet. The postmetacrista is more of a sharp edge than a raised crest as it is in *Th. cynocephalus*. It curves downwards and buccoventrally from the distolingual edge of the metacone terminating at the distalobuccal corner of the tooth, the distal end of the metastylar wing. This corner is flat and there is no trace of a raised metastyle. The buccal margin of the stylar shelf forms a raised crest that is higher than the postmetacrista, consequently the metastylar basin faces lingually as opposed to buccally as it does in *Th. cynocephalus*. The stylar crest rises as it extends mesially from the metastylar corner, ending in a well-developed stylar cusp D, which forms a mesiodistally elongate and buccolingually compressed cusp. It lies buccally and slightly distally of the metacone and is the second tallest cusp of the tooth in its present state of wear. A saddle connects stylar cusp D with the metacone that together with the metacone, separates the mesial end of the metastylar basin from the rest of the crown. The stylar crest is terminated by the ectoflexus, mesial to stylar cusp D with the latter being linked to stylar cusp B by a low, rounded saddle. A very small but deep pit is located immediately lingual to this saddle, between stylar cusp D, the metacone and stylar cusp B.

The M^3 of NTM P4326 is 2-5% larger than M^2 in all measured dimensions (Table 4), unlike the holotype specimen (Woodburne, 1967). In occlusal view there is a well-developed ectoflexus on the buccal margin between stylar cusps B and D, closer to the midlength of the tooth than in M^2. The flexure is more strongly developed than in M^2, nonetheless it is not as deep as in the M^3 of the holotype or the isolated M^3 described by Woodburne (1967). The mesial and linguodistal margins bear weakly developed constrictions between the protocone and the buccal cusps. A weakly distinct precingulum extends from the apex of stylar cusp B to a point at the base of the crown adjacent to the mesial constriction. The talon is narrower and more triangular in occlusal view than in M^2. The mesial face of the talon curves smoothly onto the occlusal surface of the talon with no preprotocrista defining its margin. The postprotocrista slopes gently down from the apex of the protocone, along the linguodistal margin of the talon. As it approaches the linguodistal surface of the metacone the crista curves sharply towards the base of the crown and a short groove separates it from the metacone. The slightly raised lingual rim of this groove is probably a vestigial metaconule. A tiny, bump-like, vestigial paraconule is present on the mesial

edge of the talon, between the protocone and the base of the paracone. There is a strong size disparity between the paracone and the metacone. In lingual view the paracone is a mere bulge on the side of the tall, pyramidal metacone. Extensive wear has removed the apex and the mesial side of the cusp, obliterating the paracristae. The base of the premetacrista forms a slightly taller, rounded blade, indicating that a carnassial notch was originally present between the postparacrista and the premetacrista.The tall conical metacone dominates the crown. Only a small wear facet is developed at its tip. The premetacrista extends steeply down the mesial face of the metacone, parallel with the mesial-distal axis of the tooth, indicating that the centrocrista was probably straight when the postparacrista component was present. The metacone is a tall conical cusp that dominates the tooth. Only a small wear facet has developed at the tip of the cusp. The postmetacrista forms a sharp edge that extends down the distal side of the metacone and then continues buccodistally as a horizontal edge along the distal margin of the metastylar wing. This part of the postmetacrista is raised slightly above the level of the buccal rim of the stylar shelf so that the metastylar basin is tilted slightly buccally unlike that of M^2. The buccodistal corner of the crown, where the postmetacrista meets the stylar crest is slightly raised producing a vestigial metastyle. The stylar crest is bowed between the metastyle and stylar cusp D in buccal view. Stylar cusp D is smaller and set lower than it is in M^2. The ectoflexus interrupts the stylar crest with a low rounded saddle joing stylar cusp D with a mesial stylar crest that rises gently to the low summit of stylar cusp B. As in M^2 there is a small pit developed lingual to the ectoflexus, adjacent to the base of the metacone.

M^4 is complete. As in other dasyuromorphians it is reduced in size relative to the preceding molars and is strongly oriented distalolingually. The metastylar wing is strongly reduced in comparison to those of the preceding molars and there is only one large cusp, the paracone, occupying the central region of the tooth, buccal to the protocone. A short but distinct parastylar crest occupies the buccomesial corner of the tooth. The buccodistal margin is evenly concave between the metastyle and the parastylar crest, rather than possessing the distinct ectoflexus seen in the preceding molars. The buccodistal face of the crown slopes strongly down to this margin from the apex of the paracone and is not offset by a stylar shelf. The mesial margin between the parastylar crest and the paracone is distinctly convex in occlusal view. The steeply sloping buccolingual face curves outward at the base of the crown in this region to form a weakly developed precingulum. Weak inflections in occlusal view separate the reduced, U-shaped protocone from the rest of the tooth. The protocone forms a small pointed tubercle that is set lower than the rest of the tooth. The lingual side of the cusp curves buccally toward the tip so that it is set away from the lingual margin and close to the groove separating the protocone from the lingual base of the paracone. The very short pre- and post- protocristae extend close to vertically down the mesial and distal edges of the buccal face of the protocone. The paracone is the largest cusp of the tooth and forms a central, pyramidal projection. A near vertically oriented wear facet occupies the mesial side of the tooth between the paracone and the parastylar crest, above the precingulum. Two elongate cristae extend from the paracone. The longest of these is the preparacrista which extends in a straight line buccomesially to the parastylar crest. In distal view the crista slopes gently down from the paracone. The shorter postparacrista extends distally to the metastyle. In lingual view this crista is slopes downward at a steep angle. The short parastylar

crest developed at the buccomesial corner of the tooth bears two minute cuspules which are presumably the parastyle and stylar cusp B.

Dentary

The dentary specimen (NTM P4327) contains the canine alveolus, roots of P_1, damaged and incomplete P_2, P_3, M_1 and M_2 and complete M_3 and M_4 (Figs. 11, 12). The anterior tip of the dentary is crushed and the tip carrying the incisors and their alveoli is missing. Posteriorly the dentary has broken off at the level of the anterior rise of the coronoid process. The dentary is relatively slender and transversely compressed, although the latter may have been accentuated by post-mortem compaction. The dentary depth below the posterior root of M_4 is 33.2 mm, which lies within the range of *Th. cynocephalus* (Table 2). The medial symphyseal surface extends posteriorly to a level near the distal end of P_3. In lateral view the anterior tip is acutely pointed and the ventral margin forms a gentle convex curve along its entire length. The ventral margin between P_2 and M_1 is expanded laterally forming a low ventrolateral torus (Fig. 12A). The lateral surface is depressed above the thickened ventral margin and bears three mental foramina below P_2, P_3 and M_2 respectively. An anterior mental foramen may be present below P_1 but crushing and fragmentation of the dentary surface in this area prevents accurate determination. Posteriorly the lateral surface of the dentary is excavated by the masseteric fossa. The ventral and anterior margins of the fossa are indistinct but it is bordered anterodorsally by a ridge that continues posterodorsally to form the leading edge of the coronoid process.

Dentary dentition

Although the incisor-bearing area is missing there is very little space between the anterior projection of the symphyseal surface and the broken anteromedial margin of the jaw tip, indicating that the incisors must have been small and crowded. The large canine was placed close to the anterior tip of the dentary and apparently projected anterodorsally. An isolated lower canine (NTM P4461) does not differ from those of *Th. cynocephalus* (Fig. 15). The cheek teeth were closely spaced with all teeth contacting their adjacent teeth except for a short diastema of 4.6 mm between P1 and P2. As in the upper tooth row of the holotype specimen the long axis of P_1 is obliquely oriented in relation to P_2 and P_3 (fig. 11B, 12B).

Only the posterior part of P_2 is preserved. It indicates a tall, buccolingually compressed triangular tooth, with a rounded distal margin that descends to the base of the crown without any expansion to form a posterior heel-like cuspid.

The apex of the central protoconid is missing from P_3. Nonetheless it is clear that it was similar to P_2 in both size and shape (Table 5). It differs in being buccolingually thicker, and having a concave posterior margin in lateral view that forms a weakly-developed heel-like posterior cuspid. A slight bulge on the anterior profile of the tooth indicates an incipient paraconid.

The central protoconid of M_1 is heavily worn but the tooth clearly displays a low rounded paraconid with a worn tip, anterior the base of the protoconid. A weak notch on the lingual side of the tooth separates the two cusps. The buccal surface of the bases of these two crowns forms a

continuous surface that faces slightly mesially and apically. The anterobuccal margin is slightly thickened to form a vague hint of a cingulid. Posterior to the paraconid is a mesiodistally short and buccolingually broad talonid shelf. The talonid is slightly wider than the trigonid (Table 6). The distal and lingual sides of the shelf are close to vertical while the buccal side forms an apicolingually sloping surface. The talonid shelf bears a flattened wear surface on its buccal side that represents a worn hypoconid. A shallow mesiodistally oriented groove separates this worn area from a low rounded entoconid developed on the lingual side of the talonid.

Most of the crown of M_2 is missing with the edges worn and rounded suggesting that this tooth was ~~lost~~ during the life of the animal. The worn talonid is slightly broader buccolingually than the talonid of M_1. No other details of this tooth are apparent.

M_3 is well preserved although the linguomesial corner of the tooth is missing, preventing determination of the height of the paraconid. A narrow but well-developed buccomesial cingulid slopes steeply distaloventrally from the mesial base of the paraconid to the base of the crown at the level of the mesial margin of the protoconid. The protoconid forms a tall, narrowly triangular cusp in lateral view. The tip is worn with an anterodorsally facing facet intersects the posterior wear facet producing a short transversely aligned crest at the tip of the protoconid. A weakly developed preprotocristid extends down the anterior surface of the protoconid to terminate at the base of the paraconid, on its buccal side. A near vertical, buccodistally facing wear facet occupies the distal surface of the protoconid. The postprotocristid forms a slightly raised carina along the lingual margin of this wear facet. The postprotocristid extends from the tip of the protoconid and terminates in the notch between the hypoconid and the protoconid. The talonid is a low, mesiodistally short shelf that is slightly wider than the trigonid. It bears two main cuspids: the hypoconid and hypoconulid, with a vestigial trace of the entoconid. The hypoconid is worn flat and its roughly circular base is set lingually from the buccal margin, resulting in a sloping buccal side of the talonid. The basal wear facet of the hypoconid lies abuts the base of the protoconid, with just a narrow notch separating them. Thus the cristid obliqua, which would have formed one half of a carnassial notch, has been obliterated. A postcristid extends a short distance from the lingual side of the hypoconid, along the distal margin of the talonid shelf to the low, pyramidal hypoconulid. Immediately lingual to the hypoconulid, at the linguodistal corner of the talonid, is a bump-like vestige of the entoconid. The lingual side of the talonid is open and the floor of the talonid basin curves downward onto the lingual side of the shelf here.

M_4 is complete and well preserved. Its mesiodistal length is greater than that of M_3 (Table 6). A well-developed, conical paraconid forms the second highest cusp of the tooth. It arises from the linguomesial corner of the tooth. The buccomesial surface is coplanar with the mesiobuccal surface of the protoconid and is bordered basally by a buccomesial cingulid, similar to that seen in M3. A sharply incised groove separates the buccodistal surface of the paraconid from the protoconid. The large protoconid is a tall, conical cusp that forms the highest point of the tooth. In buccal view it relatively taller than in *Th. cynocephalus*, with a straight as opposed to gently convex mesial margin. The groove separating the protoconid from the paraconid is narrower and far shallower than the prominent carnassial notch present in *Th. cynocephalus*. A weak preprotocristid extends from the buccal end of this groove to the apex of the protoconid. As in M^3

there is a nearly vertical wear facet developed on the distal surface of the protoconid. A distinct postprotocristid forms the lingual border of this wear facet. It extends steeply down the distal face of the protoconid and meets the postcristid described below in a small carnassial notch. The area occupied by the talonid is reduced relative to the preceding molars. A single cuspid, apparently the hypoconulid, arises from the linguodistal corner of the talonid. This forms a moderately tall conical process that stands 4.5 mm above the distal base of the crown. A short postcristid curves buccomesially from the hypoconulid to join the distal base of the protoconid. A small swelling on this cristid, where it meets the base of the protocone may represent a reduced remnant of the hypoconid. The lingual side of the talonid shelf is not bordered by any cristid or cuspid and the floor of the shelf slopes downward at its lingual side.

Discussion

Autapomorphies of *Th. potens*

Woodburne (1967) provided an extensive list of characters that distinguished *Th. potens* from *Th. cynocephalus*. Since that time an extensive range of pre-Pleistocene thylacinids have been discovered. These indicate that many of the diagnostic characters proposed by Woodburne are widely distributed among pre-Pleistocene thylacinids and represent plesiomorphic characters ~~that are general~~ for thylacinids. Other proposed diagnostic characters can now be shown to vary within *Th. potens*, with the addition of new specimens described above. The following five characters stand as unambiguous autapomorphies of *Th. potens*:

Long axis of P^1 mesiobuccally oriented in adults (modified from Murray, 1997). In occlusal view the mesiodistal axis of the first upper premolar is aligned with the canine and the subsequent premolars in most adult thylacinids including *Th. cynocephalus* (SAM M95, M1959), *Th. megiriani* (NTM P9618), *Nimbacinus dicksoni* (Wroe & Musser 2001, fig. 1b, 4) and *Badjcinus turnbulli* (Muirhead & Wroe 1998, fig. 2b). In juvenile *Th. cynocephalus* the mesial end of P^1 is rotated buccally so that the mesiodistal axis is canted mesiobuccally (SAM M1956). This is probably related to tooth crowding in juveniles since adult specimens of *Th. cynocephalus* have normally aligned first upper premolars. In contrast adult specimens of *Th. potens* have the out-turned condition.

Mesial width of the first upper molar greater than its mesial-distal length. Primitively the mesial-distal length of M^1 exceeds the mesial width (the width from the protocone to the mesiobuccal corner of the tooth) in thylacinids. This condition is present in dasyurids (e.g. *Dasyurus maculatus*: NTM U7542; *Antechinus flavipes*: NTM U7566) and all known species of thylacinids (e.g. *N. richi*: NTM P9973-11; *Th. cynocephalus*: Woodburne, 1967, table 1) except *Th. potens* (Woodburne, 1967, table 1) where the mesial width exceeds the mesial-distal length.

Reduced palatal fenestrae. As described by Woodburne (1967) the palatal fenestrae of *Th. potens* lie below the range of dimensions displayed by *Th. ~~cynocephalus~~, ~~despite coming from a larger palate~~*. Relative to the upper molar row length, the length of a palatal fenestra is about 33% in *Th.*

potens whereas this proportion ranges between 50-58% in adult *Th. cynocephalus* (pers. obs. of SAM specimens). All of the few preserved palates of other older thylacinids have relatively large palatal fenestrae like those of *Th. cynocephalus* (e.g. 55% in *Mutpuracinus archibaldi*: NTM P91168-5; 53% in *N. dicksoni*: Wroe & Musser, 2001, fig. 1b; and a fenestra that "extends from M^1 to M^3" in *B. turnbulli*: Muirhead & Wroe, 1998, p. 613). Thus the reduced condition seen in *Th. potens* is, as far as can be determined, an autapomorphy of the species.

Absence of a diastema between P_1 and P_2. Most thylacinid species possess a diastema between the first and second lower premolars, e.g. *B. turnbulli* (Muirhead & Wroe, 1998, fig. 1a), *N. dicksoni* (Wroe & Musser, 2001, fig. 2b), *Mut.archibaldi* (Murray & Megirian, 2006), *Th. macknessi* (Muirhead & Gillespie, 1995, fig. 1a) and *Th. cynocephalus* (SAM M1959). The sole known exceptions are *N. richi* (NTM P9612-4) and *Th. potens* (NTM P4327). Given that *N. richi* is phylogenetically remote from *Th. potens*, this character can be interpreted as an unambiguous autapomorphy of *Th. potens* that has convergently evolved in *N. richi*.

Relative enlargement of P_2 so that it is longer than P_3 and M_1. Primitively the longest lower premolar of thylacinids is the posterior one, here designated P_3. This condition is present in *Muribacinus gadiyuli* (Wroe, 1996, fig. 1.4), *B. turnbulli* (Muirhead & Wroe, 1998, table 2), *Mut. archibaldi* (Murray & Megirian, 2006, table 2), *N. dicksoni* (Wroe & Musser, 2001, fig. 2), *N. richi* (Murray & Megirian, 2000, table 1), *Wabulacinus ridei* (Muirhead, 1997), *Th. macknessi* (Muirhead & Gillespie, 1995, table 1), *Th. megiriani* (NTM P4376) and *Th. cynocephalus* (SAM M95, M1959). *Th. potens* is unique in having P_2 exceed P_3 in length (Table 5). Not only does P_2 exceed P_3 but it also exceeds M_1 (Table 6), indicating that it is P_2 that has undergone relative enlargement.

In addition to these characters a further pair of characters are ambiguous autapomorphies of *Th. potens* that due to their shared presence in other taxa phylogenetically close to *Th. potens* can be equally interpreted as ambiguous autapomorphies of *Th. potens* or transient synapomorphies of more inclusive clades.

Ventrally facing sulcus ventral to the maxillary root of the zygomatic arch. Both the holotype and referred maxillae of *Th. potens* possess a distinct, ventrally facing sulcus that incised along the ventral margin of the root of the zygomatic arch. In NTM P4326 this sulcus starts just above the midlength of M^3 and continues posterodorsally onto the base of the zygomatic arch, posterior to M^4. Although the posterior end of the maxilla is missing in the holotype and only known maxilla of *Th. megiriani*, the anterior end of a similar sulcus can be seen dorsal to the empty alveolus for M^4. No other thylacinids or dasyurids appear to have a comparable sulcus. It can therefore be interpreted as a convergence between *Th. potens* and *Th. megiriani*, or a transient synapomorphy of large-bodied *Thylacinus* species that was reversed in *Th. cynocephalus*.

P^2 longer than M^1. Primitively the second and third upper premolars of thylacinids have shorter crowns than the first upper molar. In *Ty. rothi*, *Th. potens* and *Th. megiriani* P^3 is enlarged so that it is longer than the first molar. This appears to be a synapomorphy of derived thylacinids including *Tyarrpecinus* and *Thylacinus* that is reversed in *Th. cynocephalus*. However it is only in

Ty. rothi and *Th. potens* that both P^2 and P^3 are longer than M^1. This is either an autapomorphy of *Th. potens* that is convergently developed in *Ty. rothi*, or it is a transient synapomorphy that is reversed in *Th. megiriani* and *Th. cynocephalus*. The presently unknown anterior upper dentitions of *W.ridei* and *Th. macknessi* would decide which one of these alternatives is the more parsimonious.

Variation within *Th. potens*

The new specimens display some distinctive differences from the original hypodigm described by Woodburne (1967). The new maxilla differs from the holotype in a number of respects, some of which resemble the modern *Th. cynocephalus*. The holotype of *Th. potens* displays a wide (4mm) diastema between the canine and P^1, whereas no such diastema is present in NTM P4326. Murray (1997) noted the anterior position of the infraorbital foramen above the posterior end of M^1 in the holotype specimen of *Th. potens* and suggested it may be related to facial shortening. However the infraorbital foramen opens above M^2 in NTM P4326 as it does in *Th. cynocephalus*. Woodburne (1967) also noted that the anterior palate of the holotype was longitudinally bowed, with a broad low ridge separating the anterior depressed area bearing the incisive foramina from the rest of the palate. The anterior palate of NTM P4326 is however simple and flat, like that of *Th. cynocephalus*. Dentally the new maxilla also displays a few differences from that of the holotype, namely the ectoflexus of M^2 is more weakly developed than that of M^3, although it is still more prominent than in the M^2 of *Th. cynocephalus*. Lastly Woodburne (1967) noted that M^2 and M^3 were subequal in size in the holotype, with M^3 being slightly shorter than M^2. In NTM P4326 M^3 exceeds M^2 in both length and width (Table 4), although the discrepancy between the two molars is not as great as that displayed by *Th. cynocephalus*.

Even more dramatic differences can be seen between Woodburne's dentary and the new dentary. As Woodburne (1967) observed, the paratype dentary fragment of *Th. potens* has an unusually deep dentary below the posterior molars, both in absolute measurements and relative to the length of the posterior molars. The depth of UCMP 66206 below M4 is 37.0 mm, or 2.4 times the length of M_4. In contrast the same measurement is 31.2 mm, or 1.8 times the length of M_4, which lies within the range displayed by *Th. cynocephalus* (Table 2). Further differences between these specimens can be seen in the teeth. Firstly, there is a well-defined precingulid on M_{3-4} of NTM P4327, whereas Woodburne (1967, pg. 35) indicated that there is "only a faint suggestion of a cingulum" in this position on the M_3 of UCMP 66206. Secondly the talonid of M_3 is not transversely reduced in NTM P4327 whereas it is distinctly narrower than the trigonid in UCMP 66206. The latter character is another feature that NTM P4327 shares with *Th. cynocephalus*.

On the basis of these comparisons it would be prudent to question whether the new specimens truly belong to *Th. potens*, or infact represent a taxon that is more closely related to *Th. cynocephalus*. The latter hypothesis is considered less likely than the former for two reasons. Firstly the new specimens share apomorphic character states with *Th. potens* that are not seen in *Th. cynocephalus*. These include: molar row lengths exceeding those of *Th. cynocephalus* (both NTM P4326 and P4327, see below); mesial end of P^1 out-turned (NTM P4326); presence of a sulcus on the ventral margin of the maxillary root of the zygomatic arch (NTM P4326); P^2 longer

than M^1 (NTM P4326). Although the type series of *Th. potens* lacked an anterior end of a dentary, the presence of an enlarged P_2 in NTM P4327 would match the derived condition of an enlarged second premolar seen in the upper dentition. In contrast, the similarities shared between these new specimens and *Th. cynocephalus* are symplesiomorphies that are general to thylacinids. Thus whatever NTM P4326 and P4327 are, their relationship appears to be closer to *Th. potens* than to any other known thylacinid. Secondly if one were to treat the new specimens as representing a second taxon then this would imply two closely-related, large-bodied apex predators living as contemporaries in the same local fauna. This is a most unlikely situation.

Thus it would appear that *Th. potens* is an unusually variable species. Given that both the new maxilla and dentary show complete eruption of all teeth and an advanced stage of tooth wear it is apparent that they represent mature individuals. Therefore ontogenetic differences are most unlikely to account for the differences in relative mandibular depth and obviously cannot account for the observed dental differences. A larger sample size is required to test the possibility that the observed variation is the result of sexual dimorphism.

Phylogenetic position of *Th. potens*

The discovery of the anterior end of the dentary of *Th. potens* revealed an unexpected plesiomorphic character state. All three premolars are set adjacent to one another, with no diastemata between them or the following M_1. Diastemata occur between P2 and P3 of all other species of *Thylacinus* but are absent from more basal thylacinids such as *W. ridei* (Muirhead, 1997), *Mut. archibaldi* (Murray & Megirian, 2006) and *B. turnbulli* (Muirhead & Wroe, 1998). A number of other previously known plesiomorphies distinguish *Th. potens* from other *Thylacinus* species these include the retention of a precingulum on M^3; M^3 that is slightly wider than it is long; and M^2 and M^3 that are subequal in length. These character states were included in a cladistic analysis to test whether the additional data was enough to cause *Th. potens* to fall outside the genus *Thylacinus*.

The analysis returned 2 most-parsimonious trees of 88 steps. The strict consensus of the two trees is well-resolved (Fig. 16A). The only polytomy encompasses the base of *Thylacinus* and the two taxa found to be most closely related to this genus, i.e. *W. ridei* and *Ma. muirheadae*. Inspection of the trees reveals that is the position of *Ma. muirheadae* that varies between the two. This is unsurprising given that this species is known from just a single tooth, making it the most poorly-known thylacinid and only scorable for 21% of the characters used in this analysis. If *Ma. muirheadae* is pruned *a posteriori* from the most parsimonious trees, a single, fully-resolved, reduced consensus tree is obtained.

The two most parsimonious trees both resolve *Th. potens* as the sister taxon to the other large-bodied late Neogene species (*Th. cynocephalus* and *Th. megiriani*) within the genus *Thylacinus* (Figure 16), supporting all previous assessments of the relationships of this species. The clade uniting the three large *Thylacinus* species has a moderate level of bootstrap support (69%) but this value is lowered by the instability of *Ma. muirheadae*. When a second bootstrap analysis is conducted, with *Ma. muirheadae* excluded, the bootstrap support for this clade jumps to 83%,

indicating it is a robust result. Thus the plesiomorphic characteristics of *Th. potens* that are listed above are interpreted as character reversals.

Size of *Thylacinus potens*

While several authors have noted the greater robustness and likely greater size of *Th. potens* relative to the modern *Th. cynocephalus* (e.g. Woodburne, 1967; only Wroe (2001) has attempted a ~~quantatitive~~ estimate of the body mass of *Th. potens*. He found the holotype specimen to have come from an individual weighing 38.7 kg but noted that the estimate was based on the combined length of M^{1-3} and an assumption of geometric similitude to *Th. cynocephalus*. The results of the size estimates for the new specimens are summarised in Table 7.

As can be seen, the different estimates for each specimen are remarkably close to one another with the exception of the estimate based upon regression of the width of M^2. The estimate of 121 kg is clearly far too high and indicates that *Th. potens* had relatively broader second upper molars in comparison to other dasyuromorphians.

It is also interesting to note that all of the estimates exceed the value of 38.7 kg that Wroe (2001) obtained for the holotype of *Th. potens* by inferring geometric similitude with Th. cynocephalus. While the estimates based on the regressions of Myers come with the caveat that they extrapolate beyond the sample used to generate the regression, they do support the hypothesis that *Th. potens* attained a larger size than the modern thylacine which had an average body weight of 29.5 kg (Paddle, 2000) and a maximum reconstructed weight of 35kg (Moeller, 1968).

However there is the additional caveat that these estimates assume that *Th. potens* had not evolved unusual body proportions that strongly departed from geometric similitude with *Th. cynocephalus* or the scaling of other dasyuromorphians. Relatively few postcranial elements for *Th. potens* are known and are still under study by the author. However, an adult humerus was recovered in Shattered Dreams close to NTM P4326 and NTM P4327 and is smaller than average for *Th. cynocephalus* and hints that the proportions of *Th. potens* may have indeed been unusual. Further study of other postcranial remains is required to determine if this humerus is typical of *Th. potens* or from an unusually small individual.

Palaeobiology

The heavy damage and wear that the teeth display, including in NTM P4326 the wearing down of P^2 to a rounded stump, the strongly blunted protocone of P^3, the virtual obliteration of the paracones from M^2 and M^3, the wearing down of M^2 to a single flat plane in NTM P4379 (Fig. 10), the virtual obliteration of the protocone by wear in NTM P4516 and the almost complete loss of the crown of M_2 in NTM P4327 (Figs. 11, 12). ~~These~~ are strongly suggestive of durophagy, quite possibly bone-cracking. However, the teeth of *Th. potens* do not show a strong trend towards bone-cracking adaptations. For example bone-cracking mammals tend to develop the following features: well developed cingula and cingulids; broad, low-crowned premolars and lower molars, lower broader molar cusps and a migration of the molar cusps toward the centre of the tooth crowns (Wroe, 1998). *Th. potens* shows no trend towards these features over the

character states present in thylacinids basally. Thus it is possible that frequent bone cracking was a relatively new behaviour in *Th. potens* and that morphological specialisations had yet been given sufficient time to evolve. Alternatively the few preserved individuals known for this species may have been exhibiting exceptional behaviour. The question can only be explored with the collection of a larger sample of specimens.

Acknowledgements

The new maxilla and dentary which form the basis of this paper were discovered in a new pit ('Shattered Dreams') which was opened thanks to the generous loan of a backhoe and licensed operator from Central Desert Shire, Northern Territory. I am deeply indebted to Glenn Marshall for making this loan possible. The specimens themselves were found and patiently excavated by Jared Archibald. I also wish to thank Catherine Kemper and Ben McHenry of the South Australian Museum for allowing me access to thylacinid specimens in their care. The photographs used in this paper were taken by Steven Jackson.

References

Archer M, Rich TH. 1982. Results of the Ray E. Lemley expeditions. *Wakaleo alcootaensis* n. sp. (Thylacoleonidae, Marsupialia), a new marsupial lion from the Miocene of the Northern Territory with a consideration of early radiation in the family. In: Archer M, ed. *Carnivorous Marsupials.* Sydney: Royal Zoological Society of New South Wales, 495-502.

Bonaparte CLJL. 1838. Synopsis vertebratorium systematis. *Nuovi Annual, Science and Nature, Bologna* 2: 105-133.

Dawson L. 1982. Taxonomic status of fossil thylacines (*Thylacinus*, Thylacinidae, Marsupialia) from late Quaternary deposits in eastern Australia. In: Archer M, ed. *Carnivorous Marsupials.* Sydney: Royal Zoological Society of New South Wales, 527-536.

Gill T. 1872. Arrangement of the families of mammals with analytical tables. *Smithsonian Miscellaneous Collections* 2: 1–98.

Megirian D. 2000. Report on shallow augering at the MAGNT Alcoota fossil reserve, June and August, 1998. *MAGNT Research Report* 7: 1-19.

Megirian D, Prideaux GJ, Murray PF, Smit N. 2010. An Australian land mammal age biochronological scheme. *Paleobiology* 36: 658-671.

Moeller H. 1968. Zur Frage der Parallelerscheinungen bei Metatheria und Eutheria. Vergleichende Untersuchungen an Beutelelwolf und Wolf. *Zeitschrift für Wissenschaftliche Zoologie* 177: 283-392

586 Muirhead J. 1992. A specialized thylacinid, *Thylacinus macknessi*, (Marsupialia: Thylacinidae)
587 from Miocene deposits of Riversleigh, northwestern Queensland. *Australian Mammalogy* 15: 67-
588 76.

589 Muirhead J. 1997. Two new Early Miocene thylacines from Riversleigh, northwestern
590 Queensland. *Memoirs of the Queensland Museum* 41: 367-377.

591 Muirhead J, Gillespie AK. 1995. Additional parts of the type specimen of *Thylacinus macknessi*
592 (Marsupialia: Thylacinidae) from Miocene deposits of Riversleigh, northwestern Queensland.
593 *Australian Mammalogy* 18: 55-60.

594 Muirhead J, Wroe S. 1998. A new genus and species, *Badjcinus turnbulli* (Thylacinidae:
595 Marsupialia), from the late Oligocene of Riversleigh, northern Australia, and an investigation of
596 thylacinid phylogeny. *Journal of Vertebrate Paleontology* 18: 612-611.

597 Murray PF. 1997. *Thylacinus megiriani*, a new species of thylacine (Marsupialia: Thylacinidae)
598 from the Ongeva Local Fauna of Central Australia. *Records of the South Australian Museum* 30:
599 43-61.

600 Murray PF, Megirian D. 1992. Continuity and contrast in middle and late Miocene vertebrate
601 communities from the Northern Territory. *The Beagle: Records of the Museums and Art Galleries*
602 *of the Northern Territory* 9: 195-218.

603 Murray PF, Megirian D. 2000. Two new genera and three new species of Thylacinidae
604 (Marsupialia) from the Miocene of the Northern Territory, Australia. *The Beagle: Records of the*
605 *Museums and Art Galleries of the Northern Territory* 16: 145-162.

606 Murray PF, Megirian D. 2006. Cranial morphology of the Miocene thylacinid *Mutpuracinus*
607 *archibaldi* (Thylacinidae, Marsupialia) and its relationships within the Dasyuromorphia.
608 *Alcheringa Special Issue* 1: 229-276.

609 Myers TJ. 2001. Prediction of marsupial body mass. *Australian Journal of Zoology* 49: 99-118.

610 Paddle R. 2000. The Last Tasmanian Tiger: the history and extinction of the thylacine.
611 Cambridge: Cambridge University Press

612 Ride, WDL. 1964. A review of Australian fossil marsupials. *Journal of the Royal Society of*
613 *Western Australia* 47: 97-131.

614 Stirton RA, Woodburne MO, Plane MD. 1967. A phylogeny of the Tertiary Diprotodontidae and
615 its significance in correlation. *Bulletin of the Bureau of Mineral Resources, Geology and*
616 *Geophysics, Australia* 85: 149-160.

617 Swofford DL. 2002. PAUP* Phylogenetic Analysis Using Parsimony (*and Other Methods).
618 Version 4. Sinauer Associates, Sunderland, MA.

Woodburne MO. 1967. The Alcoota Fauna, central Australia. *Bulletin of the Bureau of Mineral Resources Geology and Geophysics, Australia* 87: 1-187.

Wroe S. 1996. *Muribacinus gadiyuli*, (Thylacinidae: Marsupialia), a very plesiomorphic thylacinid from the Miocene of Riversleigh, northwestern Queensland, and the problem of paraphyly for the Dasyuridae (Marsupialia). *Journal of Paleontology* 70: 1032-1044.

Wroe S. 1998. A new genus and species of 'bone-cracking' daysurid (Marsupialia) from the Miocene of Riversleigh, northwestern Queensland. *Alcheringa* 22: 277-84.

Wroe S. 1999. The geologically oldest dasyurid, from the Miocene of Riversleigh, north-west Queensland. *Palaeontology* 42: 501-527.

Wroe S. 2001. *Maximucinus muirheadae*, gen. et sp. nov. (Thylacinidae: Marsupialia), from the Miocene of Riversleigh, north-western Queensland, with estimates of body weights for fossil thylacinids. *Australian Journal of Zoology* 49: 603-614.

Wroe S, Musser A. 2001. The skull of *Nimbacinus dicksoni* (Thylacinidae: Marsupialia). *Australian Journal of Zoology* 49: 487-514.

Appendix 1. Character list.

1. Relationship of jugal to infraorbital foramen: jugal widely separated from the margin of the infraorbital foramen (0); maxilla-jugal suture passes very close to the margin of the infraorbital foramen (1); jugal contributes to the posterior margin of the infraorbital foramen (2). Modified from character 3 in Muirhead and Wroe (1998). Character is treated as ordered.

2. Position of the infraorbital foramen: infraorbital foramen is dorsal to M^2 (0); infraorbital foramen is dorsal to M^1 (1). Character 12 in Murray (1997).

3. Presence or absence of a sulcus along the ventral margin of the maxillary zygomatic root: sulcus absent (0); sulcus present (1). Character is new.

4. Enclosure of the primary foramen ovale: foramen ovale partly bordered by the periotic (0); foramen ovale completely enclosed by the alisphenoid, excluding periotic from its margin (1). Character 5 in Muirhead and Wroe (1998).

5. Relationship of the alisphenoid and petrosal tympanic processes: petrosal tympanic process contacts the alisphenoid tympanic process (0); petrosal tympanic process reduced or absent, so that it does not contact the alisphenoid tympanic process (1). Character 9 in Muirhead and Wroe (1998).

6. Position of P^2: P^2 closer to P^3 than to P^1; P^2 equidistant between P^3 and P^1. Character is new.

7. Mesio-distal length of P^2: P^2 shorter than M^1; P^2 longer than M^1. Character is new.

8. Mesio-distal length of P^3: P^3 shorter than M^1; P^3 longer than M^1. Character is new.

9. Presence or absence of a distalolingual cuspule on P^3: cuspule absent (0); cuspule present (1). Character 7 in Wroe and Musser (2001).

10. Development of precingulum on M^1: precingulum present and complete extending from the mesiobuccal corner to a point mesial to the base of the protocone (0); precingulum present but incomplete, extending from mesiobuccal corner to a point mesial to the base of the paracone (1); precingulum absent (2). Character 12 in Muirhead and Wroe (1998). Character is treated as ordered.

11. Presence or absence of a precingulum on M^3: precingulum present (0); precingulum absent (1). Character is new.

12. Orientation of the preparacrista on M^1: preparacrista perpendicular to the long axis of M^1 (0); preparacrista angled mesiobuccally relative to the long axis of M^1 (1). Character 16 in Muirhead and Wroe (1998).

13. Presence or absence of a postcingulum on M^1: postcingulum present (0); postcingulum absent (1). Character 25 in Wroe and Musser (2001).

14. Development of the ectoflexus on M^2 and M^3: ectoflexus well-developed (0); ectoflexus extremely reduced or absent (1). Modified from figure 11 in Murray (1997).

15. Size of the paracone in the upper molars: large, approaching the size of the ~~khyu~~ metacone (0); significantly reduced, much less than the size of the metacone (1). Modified from character 10 in Muirhead and Wroe (1998).

16. Shape of the centrocrista of M^1 in occlusal view: sharply angled (0); obtusely angled (1); straight (2). Modified from character 15 in Muirhead and Wroe (1998). Character is treated as ordered.

17. Shape of the centrocrista of M^2 and M^3 in occlusal view: sharply angled (0); obtusely angled (1); straight (2). Modified from character 15 in Muirhead and Wroe (1998). Character is treated as ordered.

18. Elongation of the postmetacrista in upper molars: postmetacrista not elongate with the metastylar wing occupying 40-48% of the tooth length (0); postmetacrista mildly elongated with the metastylar wing occupying 48-52% of the tooth length (1); postmetacrista strongly elongated with the metastylar wing extending over 52% of the length of the tooth (2). Modified from character 14 in Muirhead and Wroe (1998). Character is treated as ordered.

19. Presence or absence of the protoconule on the upper molars: protoconule present (0); protoconule absent (1). Character 14 in Wroe and Musser (2001).

20. Presence or absence of the metaconule on the upper molars: metaconule present (0); metaconule absent (1). Character 15 in Wroe and Musser (2001).

21. Size of M^3 relative to M^2: M^3 and M^2 are subequal (0); M^3 is distinctly larger than M^2 (1). Character is new.

22. Shape of M^3: M^3 is as wide as, or wider than it is long (0): M^3 is longer than it is wide (1). Character is new.

23. Size of stylar cusp B on M^1 and M^2: stylar cusp B is well-developed (0); stylar cusp B is highly reduced or absent (1). Modified from character 11 in Muirhead and Wroe (1998).

24. Presence or absence of stylar cusp C on M^1: stylar cusp C is present (0); stylar cusp C is absent (1). Modified from character 21 in Wroe and Musser (2001).

25. Presence or absence of stylar cusp C on M^2 and M^3: stylar cusp C is present (0); stylar cusp C is absent (1). Modified from character 21 in Wroe and Musser (2001).

26. Development of stylar cusp D on M^2: stylar cusp D is present and large (0); stylar cusp D is reduced to a slight bulge or a bump (1); stylar cusp D is absent (2). Character is treated as ordered.

27. Presence or absence of stylar cusp D on M^3: stylar cusp D is present (0); stylar cusp D is absent (1). Modified from character 18 in Wroe and Musser (2001).

28. Presence or absence of stylar crest on M^3: stylar crest present (0); stylar crest absent (1). Modified from character 7 in Muirhead (1997).

29. Presence or absence of a diastema between p_1 and p_2: diastema present (0); diastema absent (1). Character 22 in Muirhead and Wroe (1998).

30. Presence or absence of a diastema between p_2 and p_3: diastema absent (0); diastema present (1). Character 23 in Muirhead and Wroe (1998)

31. Mesiodistal length of p_3 relative to p_2: p_3 longer than p_2 (0); p_3 shorter than p_2 (1). Modified from character 30 in Muirhead and Wroe (1998).

32. Presence or absence of a diastema between p_3 and m_1: diastema absent (0); diastema present (1). Character is new.

33. Development of metaconid in m_1: metaconid is a well-developed, distinct cusp (0); metaconid is reduced to a small cuspule on the side of the protoconid (1); metaconid is absent (2). Modified from character 18 in Muirhead and Wroe (1998). Character is treated as ordered.

34. Development of metaconid in M_{2-4}: metaconid is a distinct moderate-sized cusp (0); metaconid is reduced to a minute cuspule (1); metaconid is absent (2). Character 19 in Muirhead and Wroe (1998). Character is treated as ordered.

35. Position of the mesial termination of the cristid obliqua in lower molars: cristid obliqua terminates at the base of the protoconid (0); cristid obliqua extends partway up the distal side of the protoconid (1); cristid obliqua extends to the tip of the protoconid (2). Character 29 in Muirhead and Wroe (1998).Character is treated as ordered.

36. Presence or absence of a carnassial notch in the cristid obliqua of lower molars: carnassial notch absent (0); carnassial notch present (1). Character 26 in Muirhead and Wroe (1998).

37. Presence or absence of a carnassial notch in the hypocristid of lower molars: carnassial notch absent (0); carnassial notch present (1). Character 26 in Muirhead and Wroe (1998).

38. Development of the entoconid in ~~m~~$_{1-3}$: entoconid a distinct, well-developed cusp (0); entoconid an indistinct cuspule or absent altogether (1). Modified from character 20 in Muirhead and Wroe (1998).

39. Mesiodistal length of ~~m~~$_4$ relative to ~~m~~$_3$: ~~m~~$_4$ shorter than ~~m~~$_3$ (0); ~~m~~$_4$ longer than ~~m~~$_3$ (1). Character 32 in Muirhead and Wroe (1998).

40. Development of postcingulid on ~~m~~$_{1-3}$: postcingulid well-developed (0); postcingulid weakly developed (1). Character 36 in Wroe and Musser (2001).

41. Development of postcingulid on ~~m~~$_4$: postcingulid well-developed (0); postcingulid weakly developed (1). Character 37 in Wroe and Musser (2001).

42. Body size: dental measurements consistent with a body mass of less than 15 kg (0); dental measurements consistent with a body mass of 15 to 35 kg (1); dental measurements consistent with a body mass of greater than 35 kg (2). Modified from figure 11 in Murray (1997). Character is treated as ordered.

Appendix 2. Tree Description

The tree described here is the reduced strict cladistic consensus, which has had *Maximucinus muirheadae* pruned from it *a posteriori*. Designated letters for each clade respond to those in Figure 16B. Character state changes are given in brackets after each character number. Characters that have a ~~CI~~ of 1 (i.e. change only once and are free of homoplasy) are marked with an asterix.

Clade A. Thylacinidae

Content. *Muribacinus gadiyuli*, *Badjcinus turnbulli*, *Ngamalacinus timmulvaneyi*, *Mutpuracinus archibaldi, Nimbacinus dicksoni*, *Nimbacinus richi*, *Tyarrpecinus rothi*, *Wabulacinus ridei*, *Thylacinus macknessi*, *Thylacinus potens*, *Thylacinus megiriani* and *Thylacinus cynocephalus.*

Unambiguous synapomorphies. Character 9 (0 to 1): presence of a distalolingual cuspule on P^3. Reversed at clade K (acctran) or in *Th. cynocephalus* (deltran). Character 24 (0 to 1): loss of stylar cusp C on M^1.

Ambiguous synapomorphy under acctran optimisation. Character 5 (0 to 1)*: Petrosal tympanic process strongly reduced so that it does not contact the alisphenoid tympanic process. Reversed in *Mutpuracinus archibaldi*.

Clade B

Content. *Badjcinus turnbulli*, *Ngamalacinus timmulvaneyi*, *Mutpuracinus archibaldi, Nimbacinus dicksoni*, *Nimbacinus richi*, *Tyarrpecinus rothi*, *Wabulacinus ridei*, *Thylacinus macknessi*, *Thylacinus potens*, *Thylacinus megiriani* and *Thylacinus cynocephalus.*

Unambiguous synapomorphies. Character 33 (0 to 1)* Metaconid of M_1 is reduced to a small cuspule. Character 35 (0 to 1)* Mesial end of cristid obliqua extends partway up the distal slope of the protoconid.

Ambiguous synapomorphy under deltran optimisation. Character 5 (0 to 1): Petrosal tympanic process strongly reduced so that it does not contact the alisphenoid tympanic process. Reversed in *Mutpuracinus archibaldi*.

Clade C

Content. *Badjcinus turnbulli* and *Ngamalacinus timmulvaneyi.*

Unambiguous synapomorphies. Character 37 (0 to 1)*: presence of a carnassial notch in the hypocristid. Character 40 (0 to 1) presence of a posterior cingulid on M_4. Convergent in *Th. macknessi*.

Clade D

Content. *Mutpuracinus archibaldi, Nimbacinus dicksoni*, *Nimbacinus richi*, *Tyarrpecinus rothi*, *Wabulacinus ridei*, *Thylacinus macknessi*, *Thylacinus potens*, *Thylacinus megiriani* and *Thylacinus cynocephalus.*

Unambiguous synapomorphies. Character 4 (0 to 1)*: primary foramen ovale completely enclosed by the alisphenoid. Character 13 (0 to 1): loss of the postcingulum on M^1.

Clade E

Content. Mutpuracinus archibaldi, Nimbacinus dicksoni, Nimbacinus richi.

Unambiguous synapomorphy. Character 24 (1 to 0): Presence of stylar cusp C on M^1. Reversal of a character that evolved in Thylacinidae.

Clade F. Nimbacinus

Content. Nimbacinus dicksoni, Nimbacinus richi.

Unambiguous synapomporphy. Character 30 (0 to 1): Presence of a diastema between P_2 and P_3. Convergent in *Muribacinus gadiyuli*, and in *Thylacinus* with a reversal in *Th. potens* (acctran), or convergent in *Thylacinus macknessi* and clade K (deltran).

Clade G

Content. *Tyarrpecinus rothi*, *Wabulacinus ridei*, *Thylacinus macknessi*, *Thylacinus potens*, *Thylacinus megiriani* and *Thylacinus cynocephalus.*

Unambiguous synapomorphies. Character 8 (0 to 1): P^3 longer than M^1. Reversed in *Th. cynocephalus*. Character 16 (0 to 1)*: Wide, obtuse angle between the postparacrista and premetacrista of M^1, creating a nearly straight centrocrista. Character 18 (0 to 1)*: mild elongation of the postmetacrista in M^2 and M^3 so that it is greater than 48% of the total length of the tooth. Character 38 (0 to 1)*: Loss of a distinct entoconid.

Ambiguous synapomorphies under acctran optimisation. Character 7 (0 to 1): P^2 longer than M^1 Reversed in clade K. Character 10 (0 to 1): Reduction of the precingulum of M^1 to an incomplete cingulum that does not reach the talon. Reversed to complete precingulum in *Thylacinus,* and then reduced to total loss in clade K. Chartacter 20 (0 to 1): Loss of metaconule on M^1 to M^3. Reversed in *Thylacinus* and then lost again in clade K. Character 33 (1 to 2): Metaconid of M_1 entirely lost. Convergent in *B. turnbulli*. Character 40 (0 to 1)*: Loss of postcingulid on M_1 to M_3. Character 34 (0 to 1)*: Reduction of metaconids on M_2 to M_4 to minute cuspules. Character 3 (0 to 1): Presence of a sulcus on the ventral margin of the maxillary root of the zygomatic arch. Reversed in *Th. cynocephalus*.

Clade H

Content. *Wabulacinus ridei*, *Thylacinus macknessi*, *Thylacinus potens*, *Thylacinus megiriani* and *Thylacinus cynocephalus.*

Unambiguous synapomorphies. Character 12 (0 to 1)*: preparacrista on M^1 is angled mesiobuccally. Character 16 (1 to 2)*: Centrocrista of M^1 is straight and parallel with mesiodistal axis of the tooth. Character 17 (0 to 1)*: Wide, obtuse angle between the postparacrista and premetacrista of M^2 and M^3, creating a nearly straight centrocrista. Character 19 (0 to 1): Loss of protoconule on upper molars. Convergent in *Nimbacinus richi*. Character 23 (0 to 1): Stylar cusp B on M^1 is highly reduced to absent. Convergent in *Badjcinus turnbulli*. Character 25 (0 to 1): Loss of stylar cusp C on M^2 and M^3. Convergent in *Muribacinus gadiyuli*.

Ambiguous synapomorphies under Deltran optimisation. Character 40 (0 to 1)*: Loss of postcingulid on M_1 to M_3. Character 34 (0 to 1)*: Reduction of metaconids on M_2 to M_4 to minute cuspules.

Clade I. *Thylacinus*

Unambiguous synapomorphy. Character 36 (0 to 1) presence of a carnassial notch in the cristid obliqua. Convergent in *Ngamalacinus timmulvaneyi.*

Ambiguous synapomorphies under deltran optimisation. Character 33 (1 to 2): Complete loss of metaconid on M_1. Convergent in *Badjcinus turnbulli*.

Ambiguous synapomorphies under acctran optimisation. Character 1 (0 to 1): Maxilla-jugal suture passes very close to the margin of the infraorbital foramen so that only a thin sliver of the maxilla separates the jugal from the foramen. Convergent in *Ngamalacinus timmulvaneyi*. Character 10 (1 to 0): Presence of a complete precingulum on M^1. Reversal of a character that was incompletely lost at clade G. Character 17 (1 to 2)*: Straight centrocrista on M^2 and M^3. Character 18 (1 to 2)*: Extreme elongation of the postmetacrista so that it is over 52% of the length of the tooth. Character 20 (1 to 0): Presence of a metaconule on the upper molars. Reversal of a character that was lost at clade G. Character 30 (0 to 1): Presence of a diastema between P_2 and P_3. Convergent in *Thylacinus macknessi*, *Nimbacinus* and *Muribacinus gadiyuli*.

Clade J

Content. *Thylacinus potens*, *Thylacinus megiriani* and *Thylacinus cynocephalus.*

Unambiguous synapomorphies. Character 15 (0 to 1): Paracone of upper molars significantly reduced in comparison to metacone. Convergent in *Tyarrpecinus rothi*. Character 34 (1 to 2)*: metaconids of M_2 to M_4 completely lost. Character 35 (1 to 2)*: mesial end of cristid obliqua extends to the tip of the protoconid. Character 39 (0 to 1): M_4 is longer than M_3. Convergent in *Mutpuracinus archibaldi*. Character 42 (0 to 1): Increased body mass, so that it is greater than 15 kg.

Ambiguous synapomorphies under deltran optimisation. Character 1 (0 to 1): Maxilla-jugal suture passes very close to the margin of the infraorbital foramen so that only a thin sliver of the maxilla separates the jugal from the foramen. Convergent in *Ngamalacinus timmulvaneyi*. Character 17 (1 to 2)*: Straight centrocrista on M^2 and M^3. Character 18 (1 to 2)*: Extreme elongation of the postmetacrista so that it is over 52% of the length of the tooth.

Clade K

Content. *Thylacinus megiriani*, *Thylacinus cynocephalus*.

Unambiguous synapomorphies. Character 10 (0 to 2)*: complete loss of precingulum on M^1. Character 11 (0 to 1)*: loss of precingulum on M^3. Character 21 (0 to 1)*: M^3 greater than 5% longer than M^2. Character 22 (0 to 1)*: M^3 is longer than it is wide. Character 28 (0 to 1)*: loss of stylar crest on M^3. Character 32 (0 to 1)*: Presence of a diastema between P_3 and M_1.

Ambiguous synapomorphies under deltran optimisation. Character 20 (0 to 1): loss of metaconule on upper molars. Convergent in *Tyarrpecinus rothi* and *Wabulacinus ridei*. Character 30 (0 to 1): Presence of a diastema between P_2 and P_3. Convergent in *Muribacinus gadiyuli*, *Nimbacinus* and *Thylacinus macknessi*.

Ambiguous synapomorphies under acctran optimisation. Character 7 (1 to 0). P^2 is shorter than M^1. Reversal of a character that evolved in clade G. Character 9 (1 to 0). Loss of distalolingual cusp on P^3. Reversal of a character that evolved in Thylacinidae.

Figure 1

Locality Map

Figure 1. Map of north-west corner of Alcoota Fossil Reserve showing the principal excavation sites of the Alcoota Local Fauna.

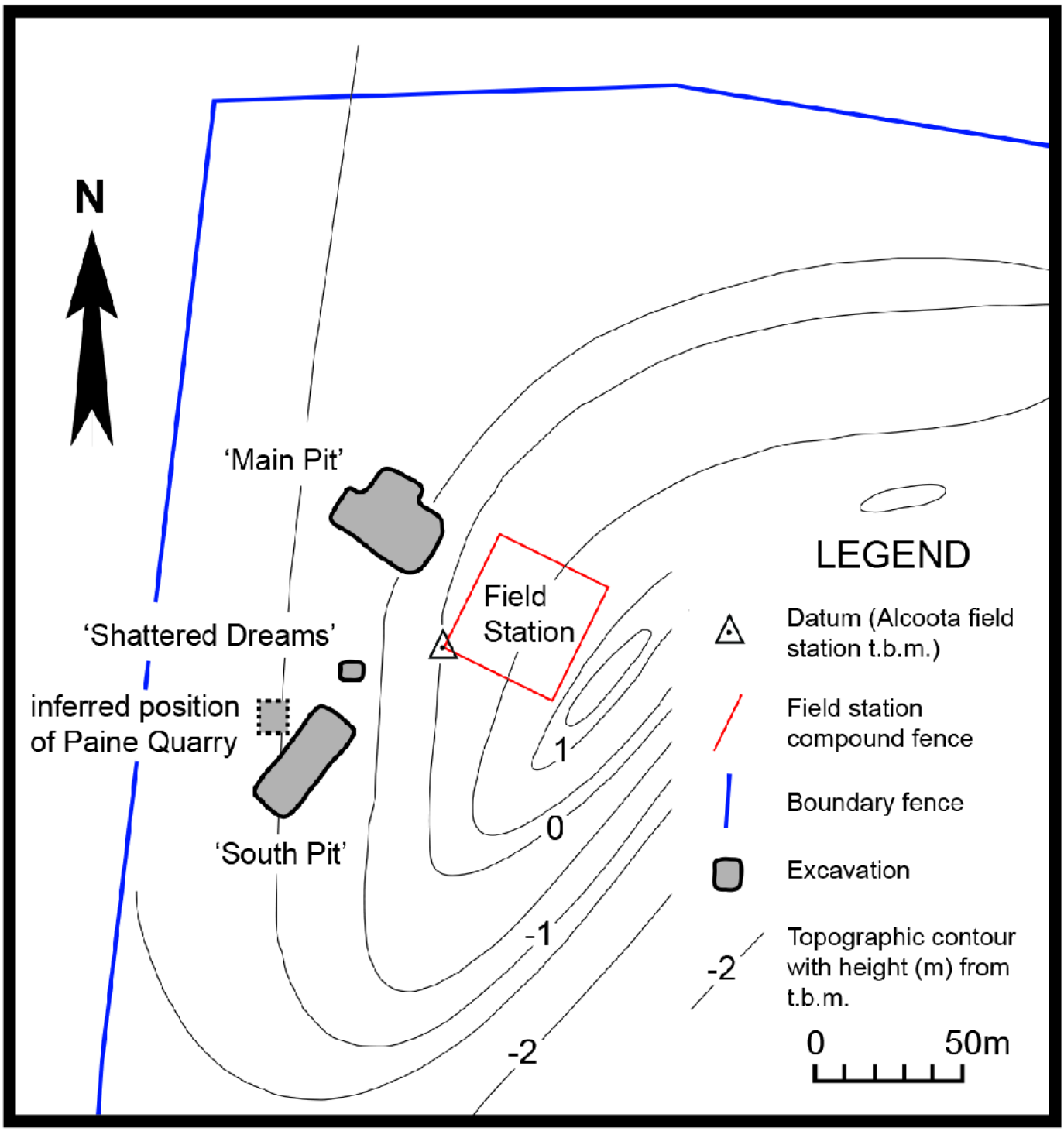

Figure 2

Whole maxilla

Figure 2. *Thylacinus potens*. NTM P4326, right maxilla. **A**, lateral view. **B**, ventral view. **C**, reconstruction of palate by mirror imaging the right side. Abbreviations: Ca, canine alveolus; if, incisive foramen; iof, infraorbital foramen; M1-4, molars 1-4; P1-3, premolars 1-3; pf, palatine fenestra; sym, symphyseal surface. Scale bars = 50 mm.

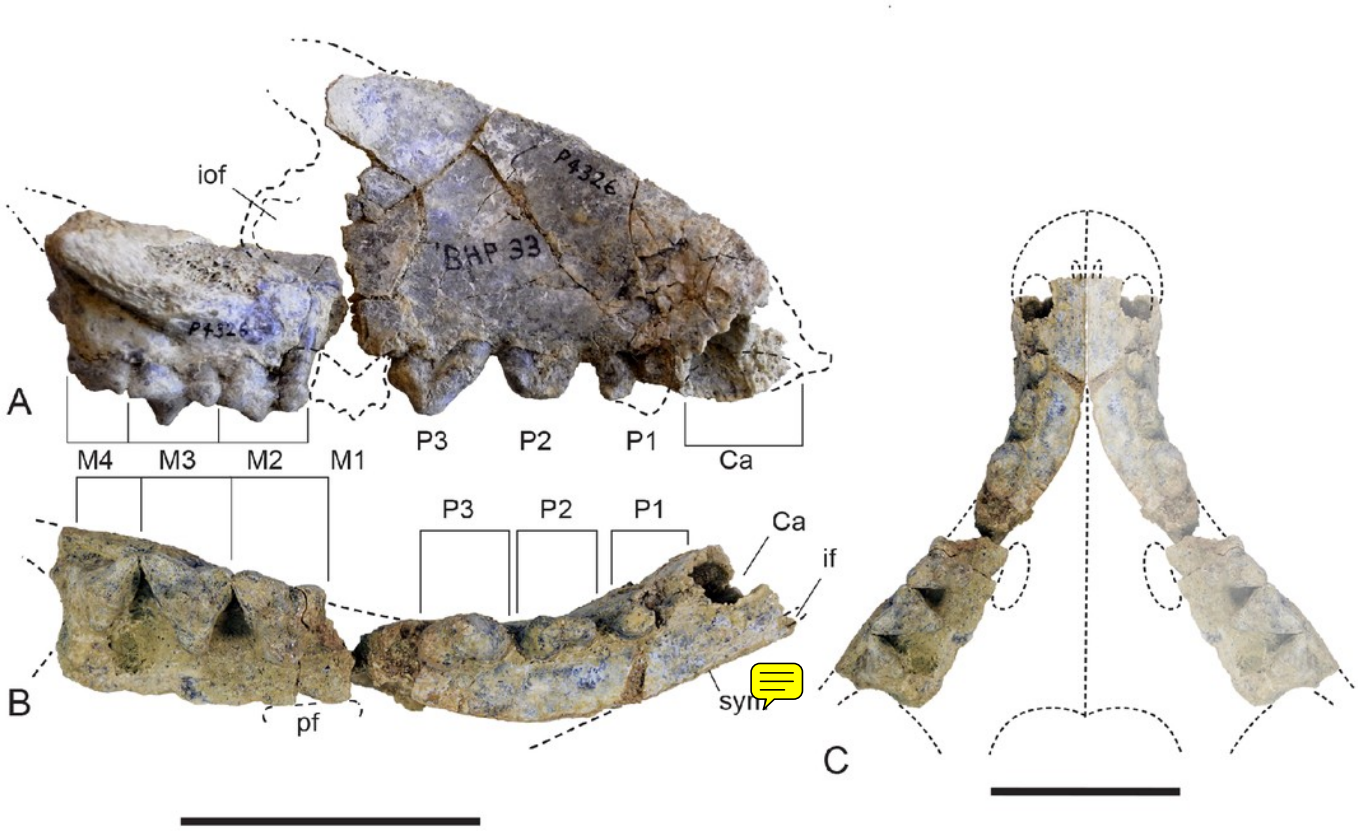

Figure 3

Photographs of anterior maxilla fragment

Figure 3. *Thylacinus potens*. NTM P4326, detail of the anterior fragment of the right maxilla. **A**, lateral view. **B**, ventral view. **C**, medial view. Scale bar = 20 mm.

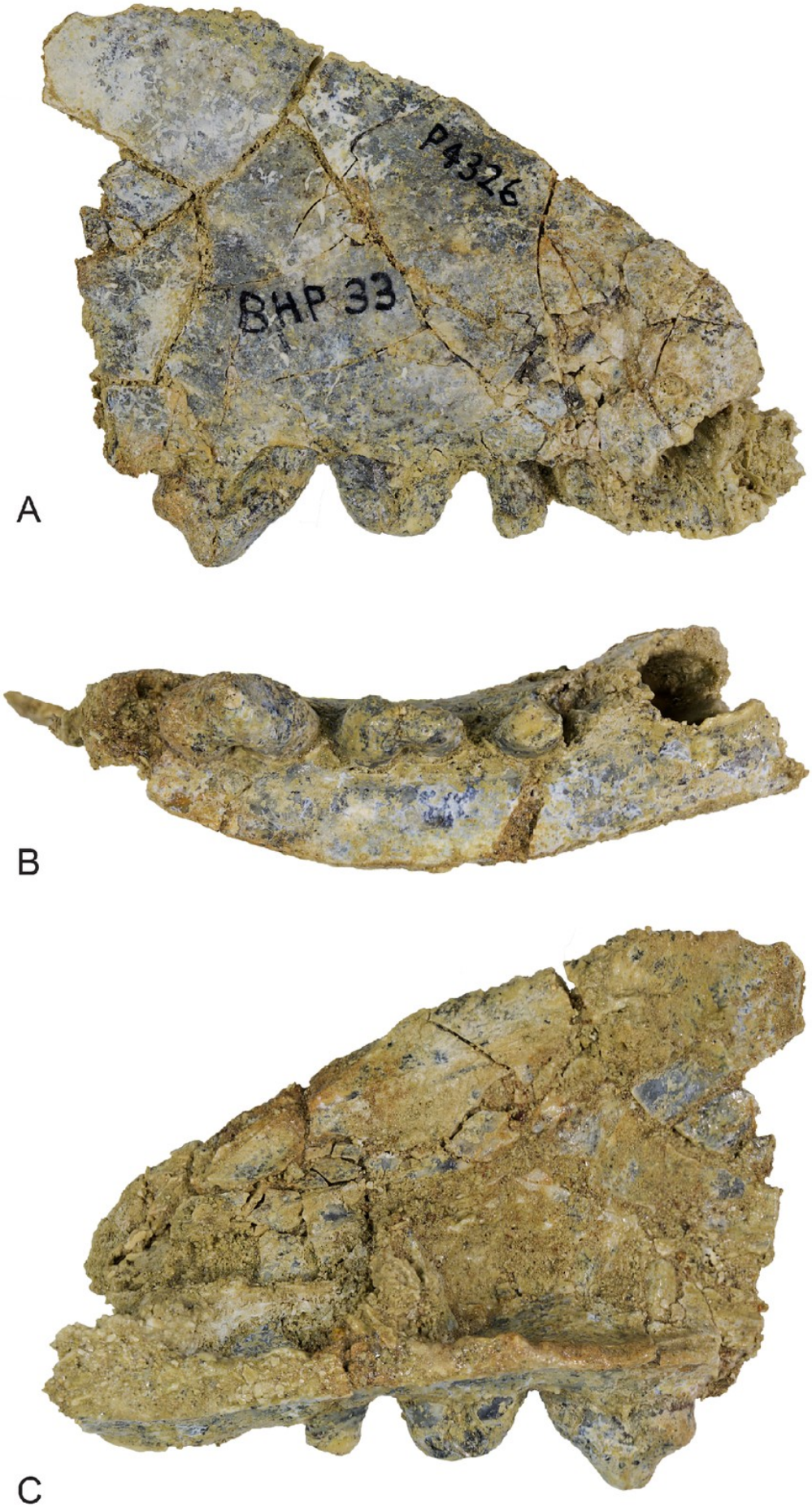

Figure 4

Drawings of anterior maxilla fragment.

Figure 4. *Thylacinus potens*. NTM P4326, anterior fragment of the right maxilla, interpretive drawings of the photographs in figure 3. **A**, lateral view. **B**, ventral view. **C**, medial view. Abbreviations: an, articulation surface for nasal; apm, articulation surface for premaxilla; bh, basal heel; Ca, canine alveolus; dr, distal root; drP1-3; distal root of premolars 1-3; if, incisive foramen; mp, palatal shelf of the maxilla; mr, mesial root; mra, alveolus of the mesial root; mrP1-3, mesial roots of premolars 1-3; pr, protocone; sym, symphyseal surface. Grey fill represent areas of adherent matrix, areas hatched with continuous horizontal lines represent broken bone and tooth surfaces. Scale bar = 30 mm.

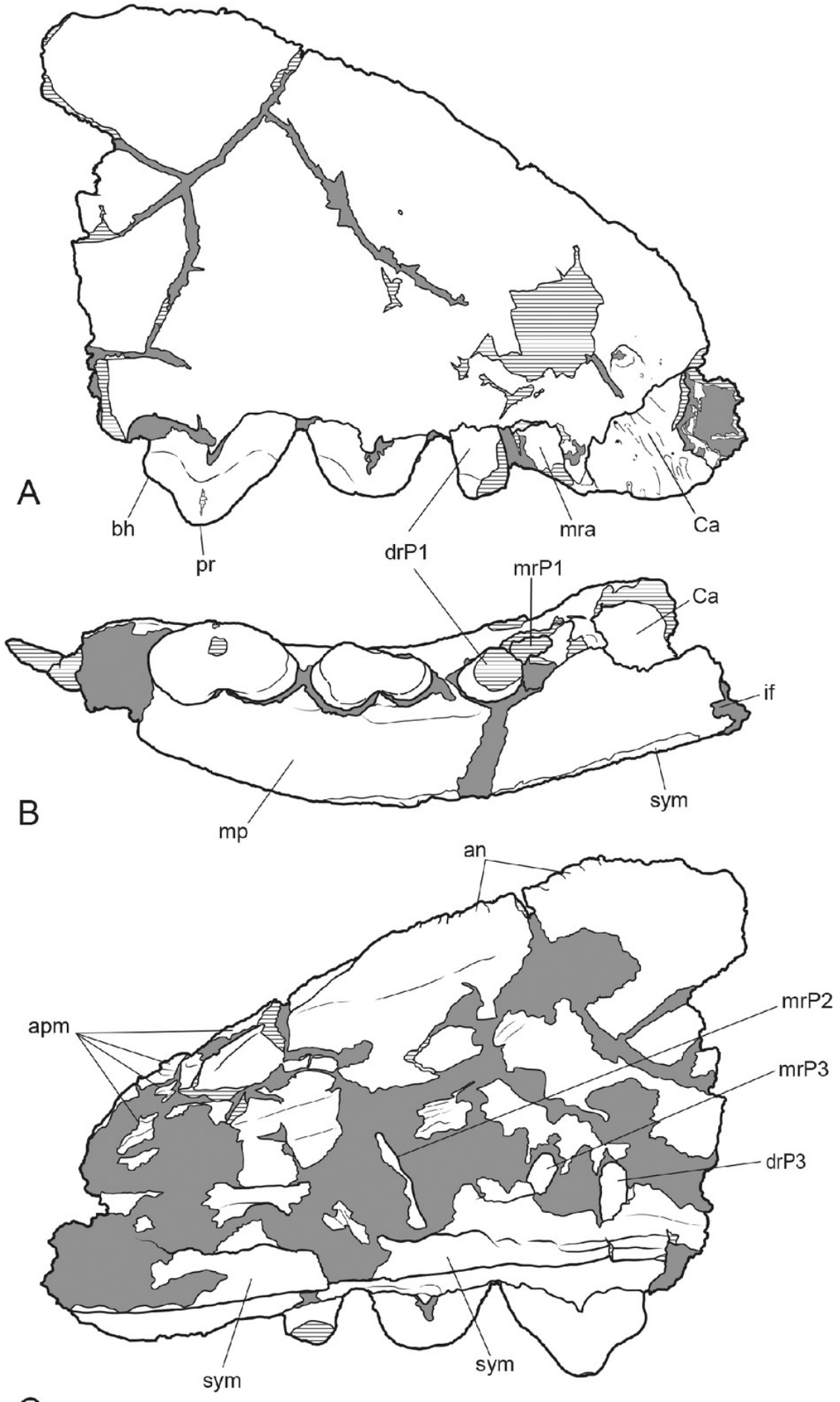

Figure 5

Lateral and medial views of posterior maxilla fragment.

Figure 5. *Thylacinus potens*. NTM P4326, detail of the posterior fragment of the right maxilla. **A**. lateral view. **B**, interpretive drawing of A. **C**, medial view. **D**, interpretive drawing of C. Abbreviations: aj, articulation surface for jugal; ap, articulation surface for palatine; ioc, infraorbital canal; me, metacone; mpf, margin of the palatal fenestra; ms, metastyle; pa, paracone; pr, protocone; ps, parastyle; sB, stylar cusp B; sD, stylar cusp D. Arrow indicates the level of the posterior margin of the infraorbital foramen. Grey fill represent areas of adherent matrix, areas hatched with continuous horizontal lines represent broken bone and tooth surfaces. Scale bar = 30 mm.

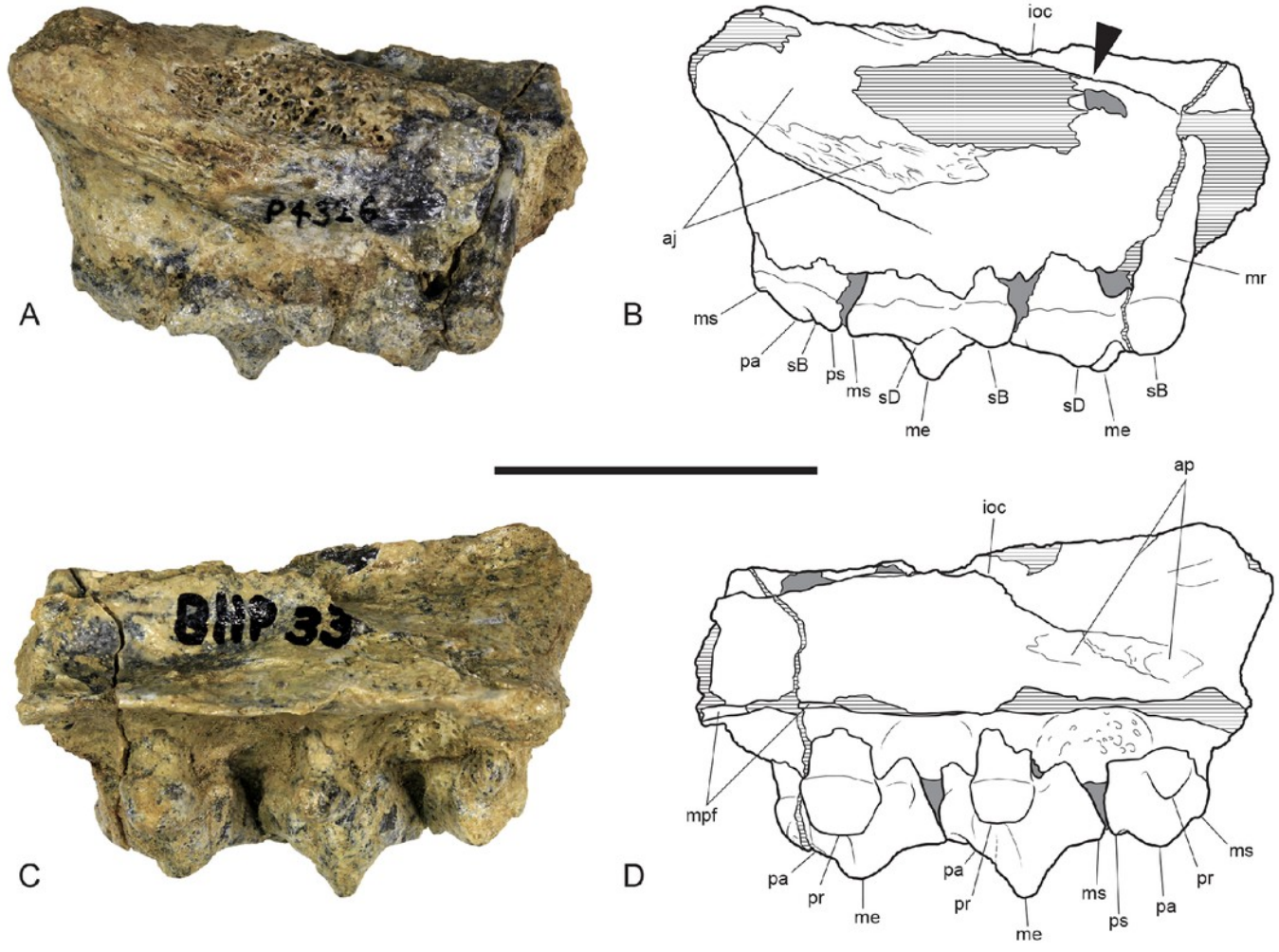

Figure 6

Photographs of posterior maxilla fragment in dorsal, ventral, anterior and posterior views.

Figure 6. *Thylacinus potens*. NTM P4326, detail of the posterior fragment of the right maxilla. **A**. ventral view. **B**, anterior view. **C**, dorsal view. **D**, posterior view. Scale bar = 30 mm.

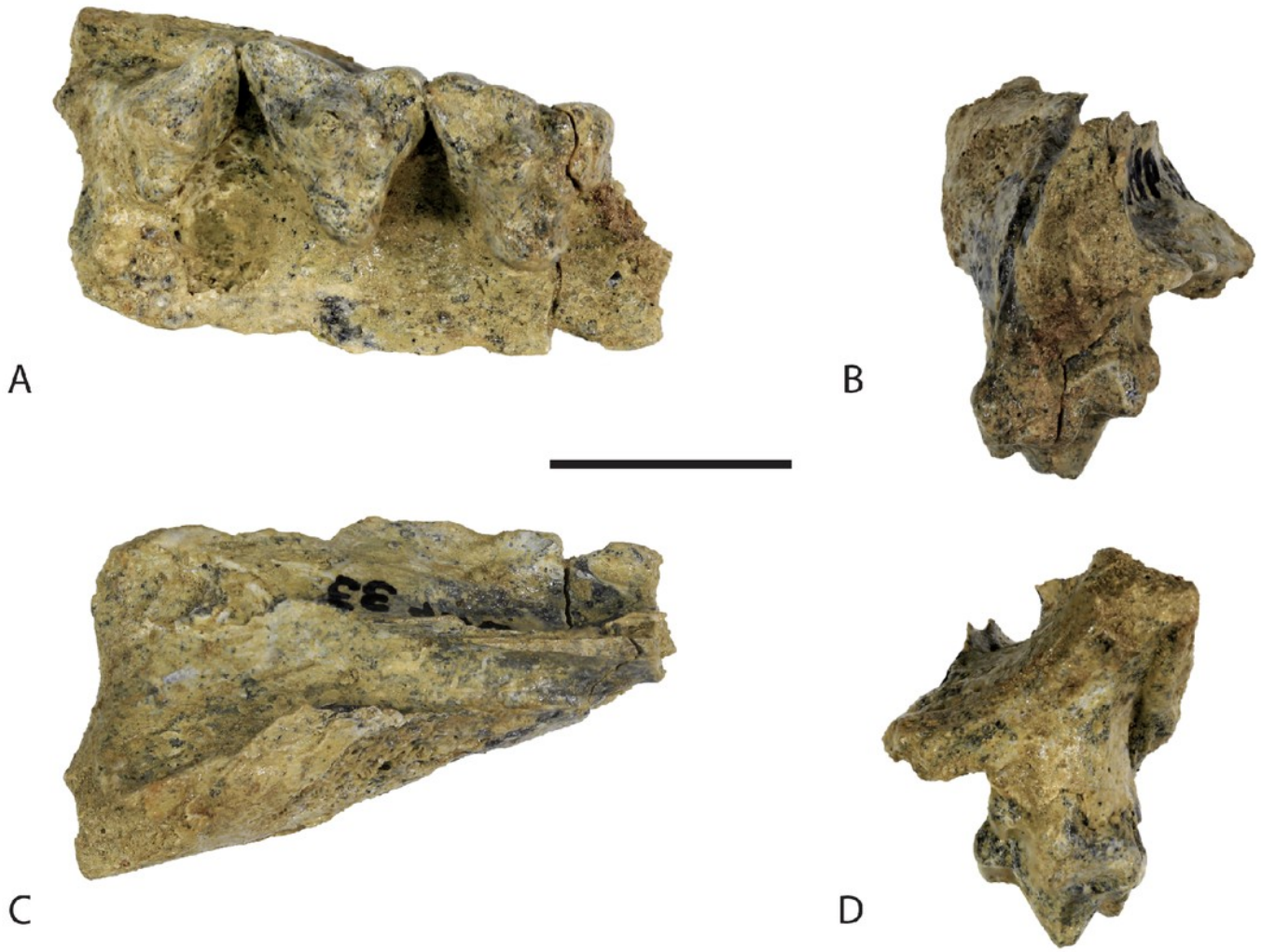

Figure 7

Drawings of posterior maxilla fragment in dorsal, ventral, anterior and posterior views.

Figure 7. *Thylacinus potens*. NTM P4326, posterior fragment of the right maxilla, interpretive drawings of the photographs in figure 6. **A**. ventral view. **B**, anterior view. **C**, dorsal view. **D**, posterior view. Abbreviations: aj, articulation surface for jugal; ap, articulation surface for palatine; ioc, infraorbital canal; me, metacone; mpf, margin of the palatal fenestra; ms, metastyle; pa, paracone; pr, protocone; ps, parastyle; sB, stylar cusp B; sD, stylar cusp D; vs, ventral sulcus. Grey fill represent areas of adherent matrix, areas hatched with continuous horizontal lines represent broken bone and tooth surfaces. Scale bar = 30 mm.

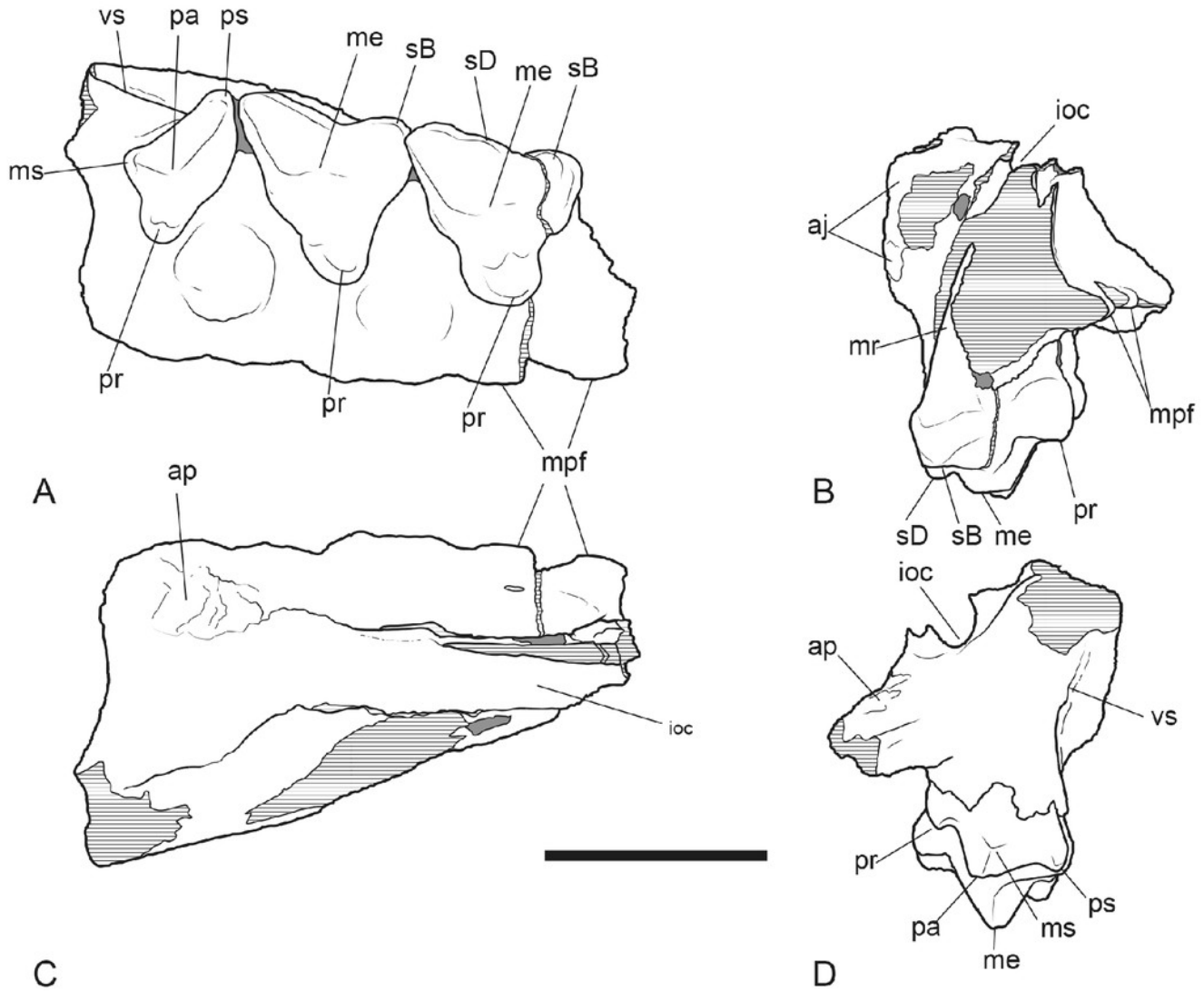

Figure 8

Upper molars in occlusal view

Figure 8. *Thylacinus potens*. NTM P4326, detail of upper molar tooth row in occlusal view. **A**, photograph. **B**, interpretive drawing of A. Abbreviations: ef, ectoflexus; me, metacone; ms, metastyle; pa, paracone; pc, precingulum; pmc, postmetacrista; ppc, postparacrista; pprc, postprotocrista; pr, protocone; prpc, preparacrista; ps, parastyle; sB, stylar cup B; sD, stylar cusp D. Areas hatched with continuous horizontal lines represent broken tooth surfaces, areas hatched with discontinuous lines represent wear surfaces. Scale bar = 20 mm.

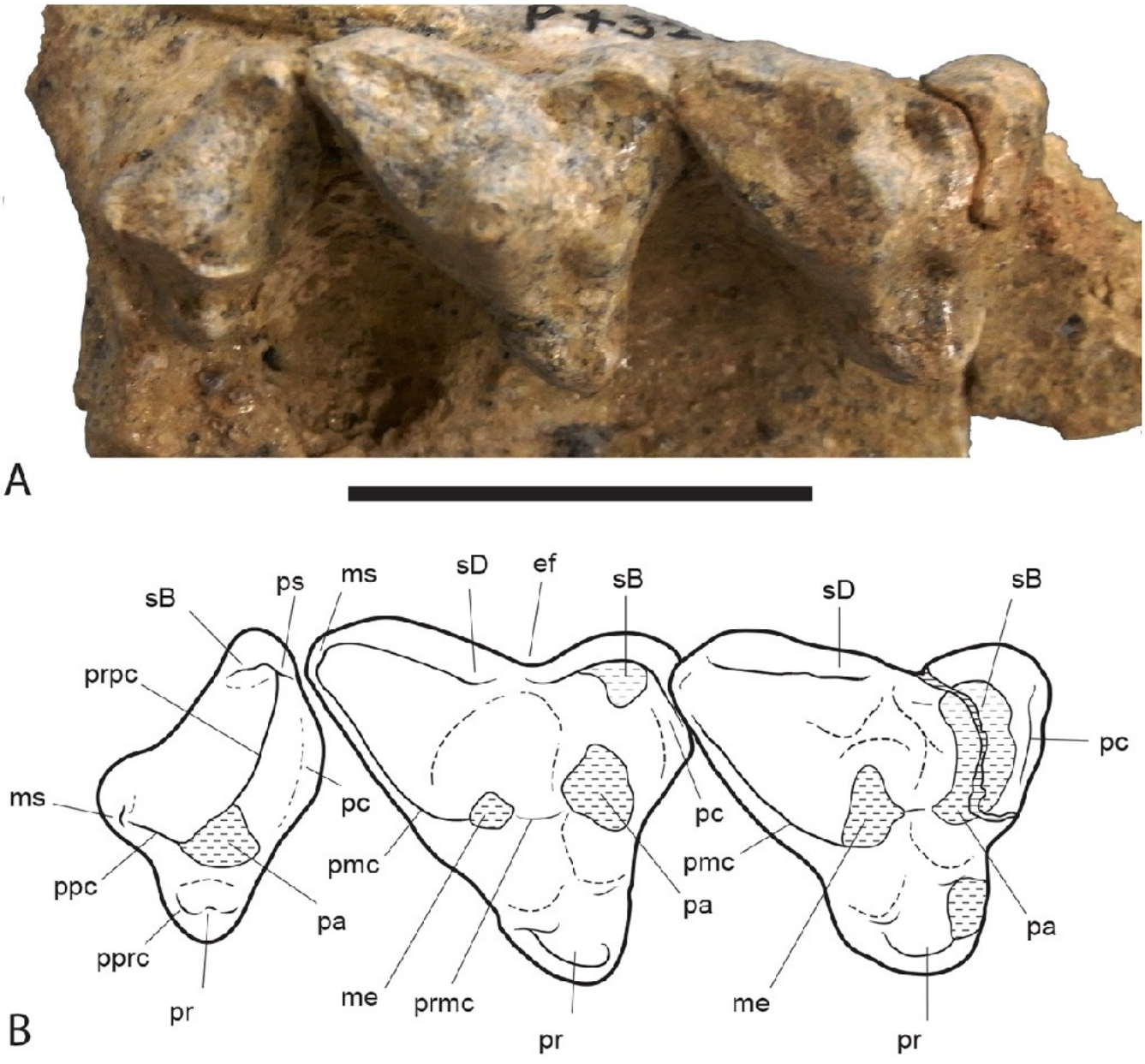

Figure 9

Isolated upper premolar

Figure 9. *Thylacinus potens*. NTM P4332, isolated left P^3. A, buccal view. B, occlusal view. C, lingual view. D, interpretive drawing of A. E, interpretive drawing of B. F, interpretive drawing of C. Abbreviations: bh, basal heel; dlcl, distalolingual cuspule; dr, distal root; mr, mesial root; pr protocone. Grey fill represent areas of adherent matrix, areas hatched with continuous horizontal lines represent broken tooth surfaces, areas hatched with discontinuous lines represent wear surfaces. Scale bar = 10 mm.

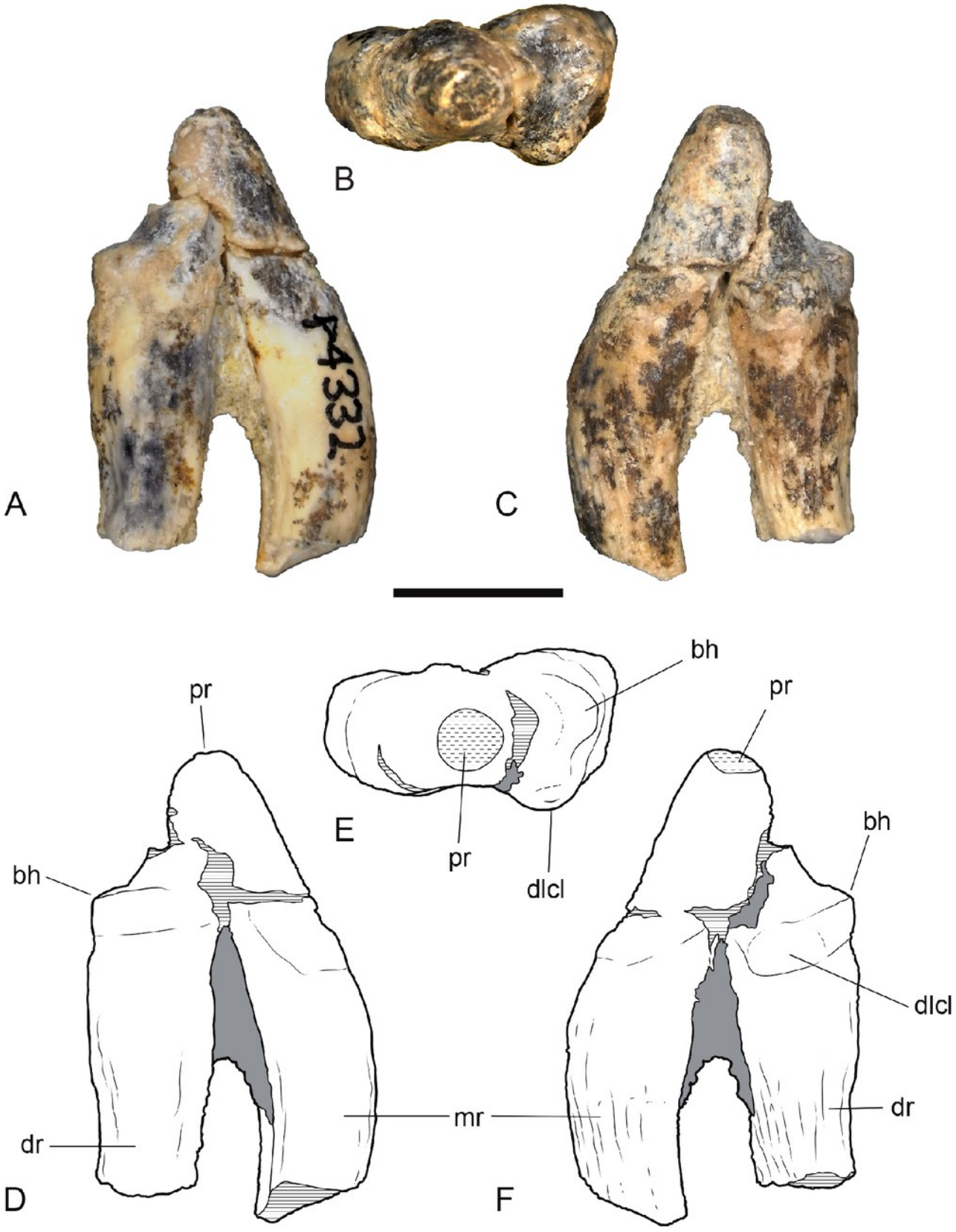

Figure 10

Heavily worn upper molar

Figure 10. *Thylacinus potens*. NTM P4379, heavily worn right M^2 in a fragment of the right maxilla. **A**, ~~photograph of~~ occlusal view. **B**, ~~photograph of~~ buccal view. **C**, ~~photograph of~~ lingual view. **D**, interpretive drawing of A. **E**, interpretive drawing of B. **F**, interpretive drawing of C. Abbreviations: dbr, distal buccal root; ef, ectoflexus; lr, lingual root; mbr, mesial buccal root; ms, metastyle; mx, maxilla fragments; pc, precingulum; pr, protocone; sB, stylar cusp B. Grey fill represent areas of adherent matrix, areas hatched with continuous horizontal lines represent broken tooth surfaces, areas hatched with discontinuous lines represent wear surfaces. Scale bar = 10 mm.

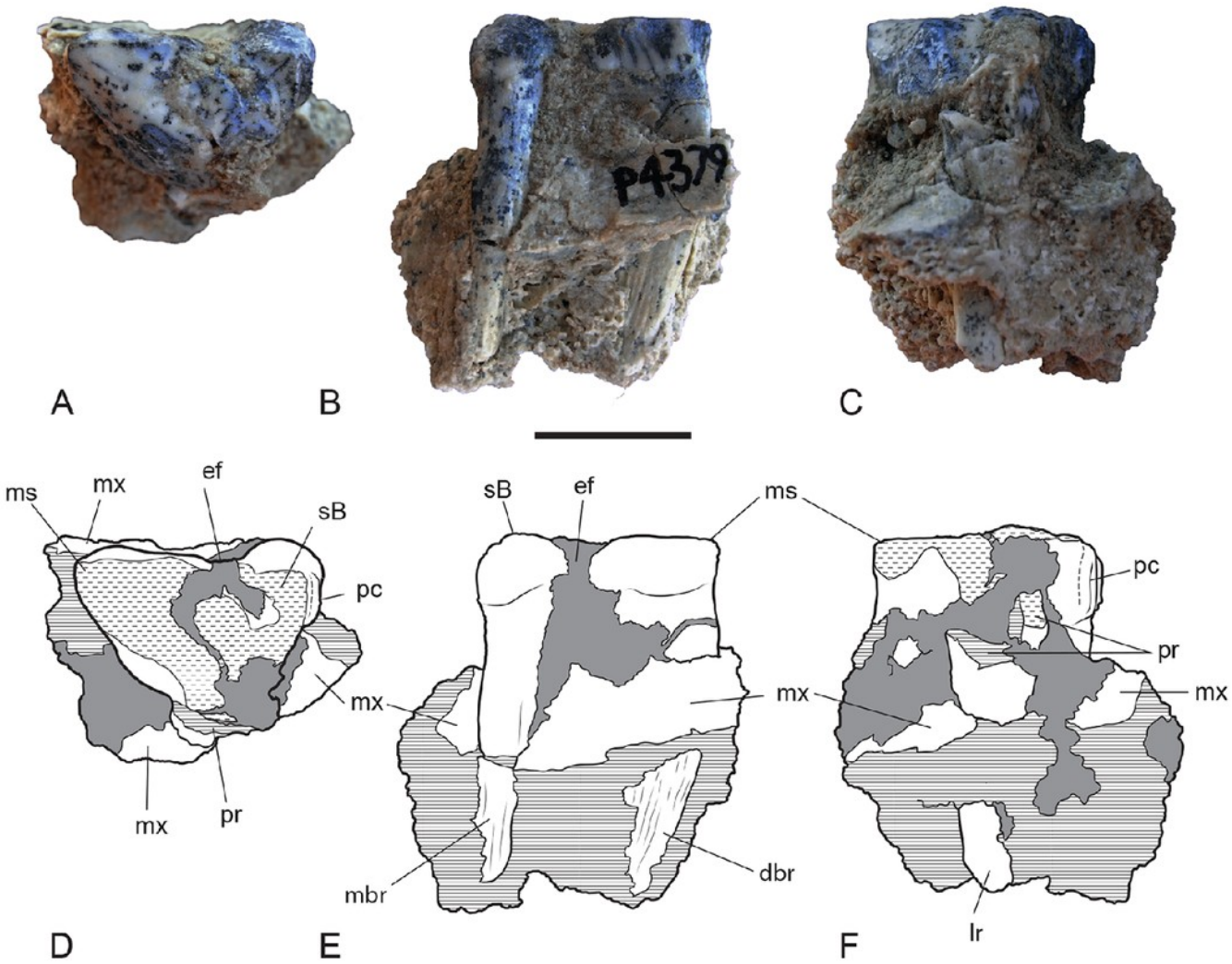

Figure 11

Photographs of dentary

Figure 11. *Thylacinus potens*. NTM P4327, ~~photographs of~~ horizontal ramus of left dentary. **A**, lateral view. **B**, occlusal view. **C**, medial view. Scale bar = 50 mm.

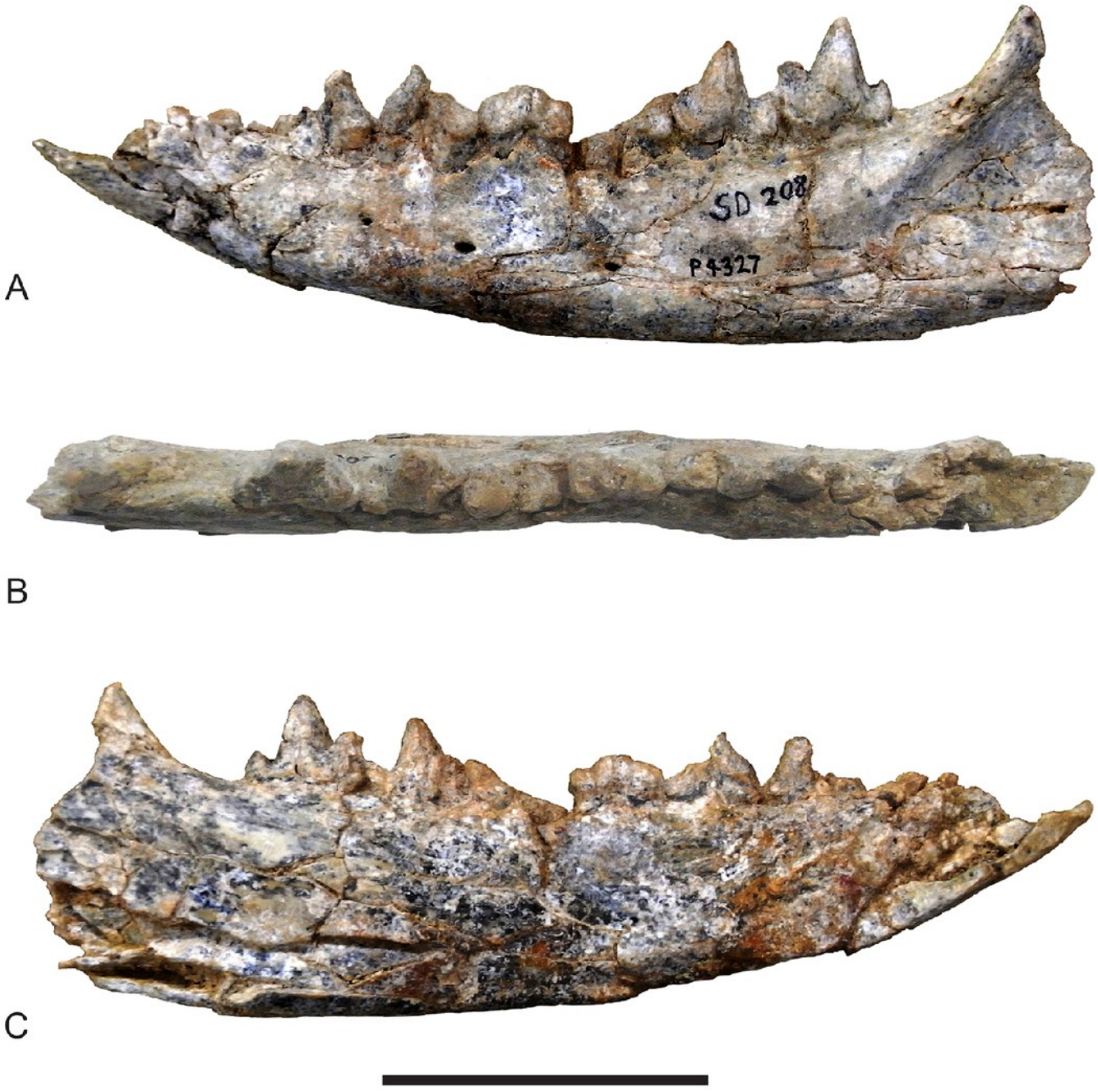

Figure 12

Drawings of dentary

Figure 12. *Thylacinus potens*. NTM P4327, interpretive drawings of figure 11. **A**, lateral view. **B**, occlusal view. **C**, medial view. Abbreviations: ca, lower canine alveolus; df, digastric fossa; drp1, distal root of first premolar; m1-4, molars 1 to 4; mf, masseteric fossa; mrp1, mesial root of first premolar; p1-3, premolars 1 to 3; pmf, posterior mental foramina; sym, symphyseal surface; vt, ventrolateral torus. Grey fill represent areas of adherent matrix, areas hatched with continuous horizontal lines represent broken bone and tooth surfaces, areas hatched with discontinuous lines represent wear surfaces. Scale bar = 50 mm.

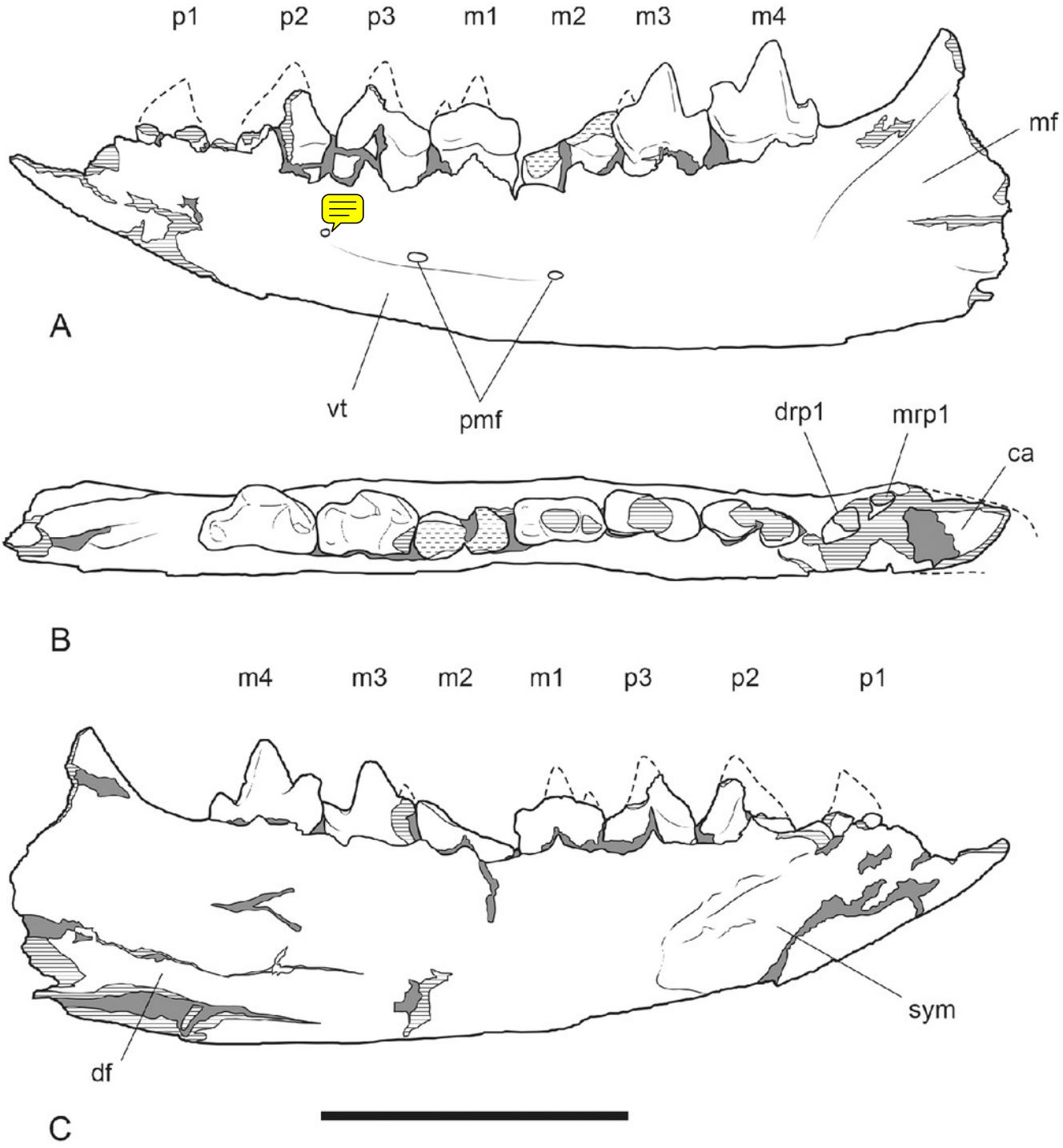

Figure 13

lower molars in occlusal view

Figure 13. *Thylacinus potens*. NTM P4327, detail of lower molar tooth row in occlusal view. **A**, posterior molars. **B**, first molar. **C**, interpretive drawing of A. **D**, interpretive drawing of B. Abbreviations: cdo, cristid obliqua; cn, carnassial notch; ed, entoconid; hd, hypoconid; pad, paraconid; pcd, postcristid; pcid, precingulid; ppcd, postparacristid; prd, protoconid; prpcd, preprotocristid. Grey fill represent areas of adherent matrix, areas hatched with continuous horizontal lines represent broken tooth surfaces, areas that are hatched with discontinuous lines represent wear surfaces. Scale bar = 20 mm.

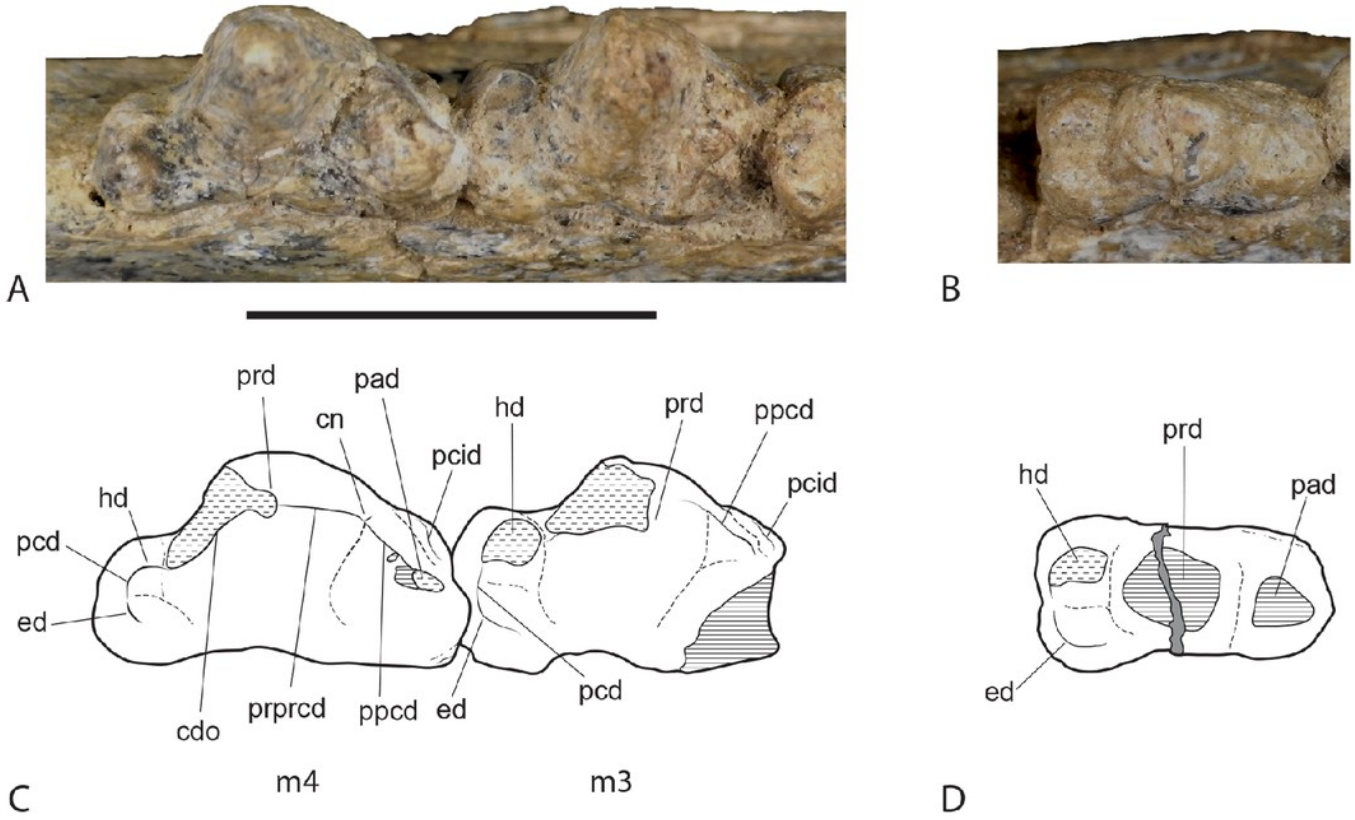

Figure 14

Lower molars in buccal view.

Figure 14. *Thylacinus potens*. NTM P4327, detail of lower molar tooth row in buccal view. Abbreviations: cdo, cristid obliqua; cn, carnassial notch; ed, entoconid; hd, hypoconid; pad, paraconid; pcd, postcristid; pcid, precingulid; prd, protoconid; prpcd, preprotocristid. Grey fill represent areas of adherent matrix, areas hatched with continuous horizontal lines represent broken tooth surfaces, areas that are hatched with discontinuous lines represent wear surfaces. Scale bar = 20 mm.

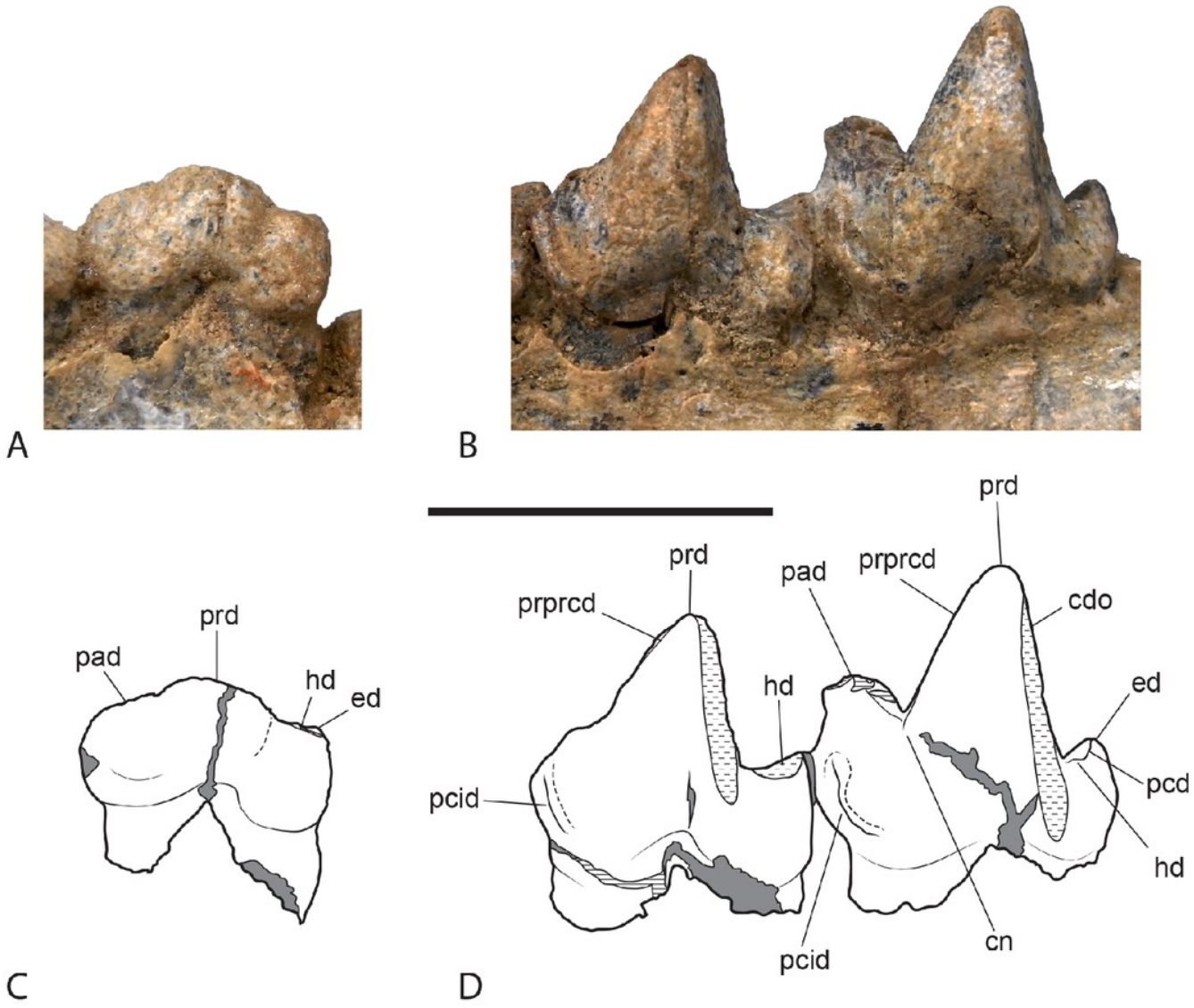

Figure 15

isolated lower canine

Figure 15. *Thylacinus potens*. NTM P4461, right lower canine. A, buccal view. B, distal view. Scale bar = 10 mm.

Figure 16

Cladograms of thylacinid phylogeny

Figure 16. Consensus trees of two most-parsimonious-trees (tree length = 88 steps) resulting from a cladistic analysis of 13 thylacinid taxa with Dasyuridae set as the user-defined outgroup. **A**, strict consensus with bootstrap support values for clades with support values >50 %. **B**, fully resolved reduced cladistic consensus obtained after *a posteriori* pruning of *Maximucinus muirheadae*. Letters at nodes correspond to those in the tree description in Appendix 2.

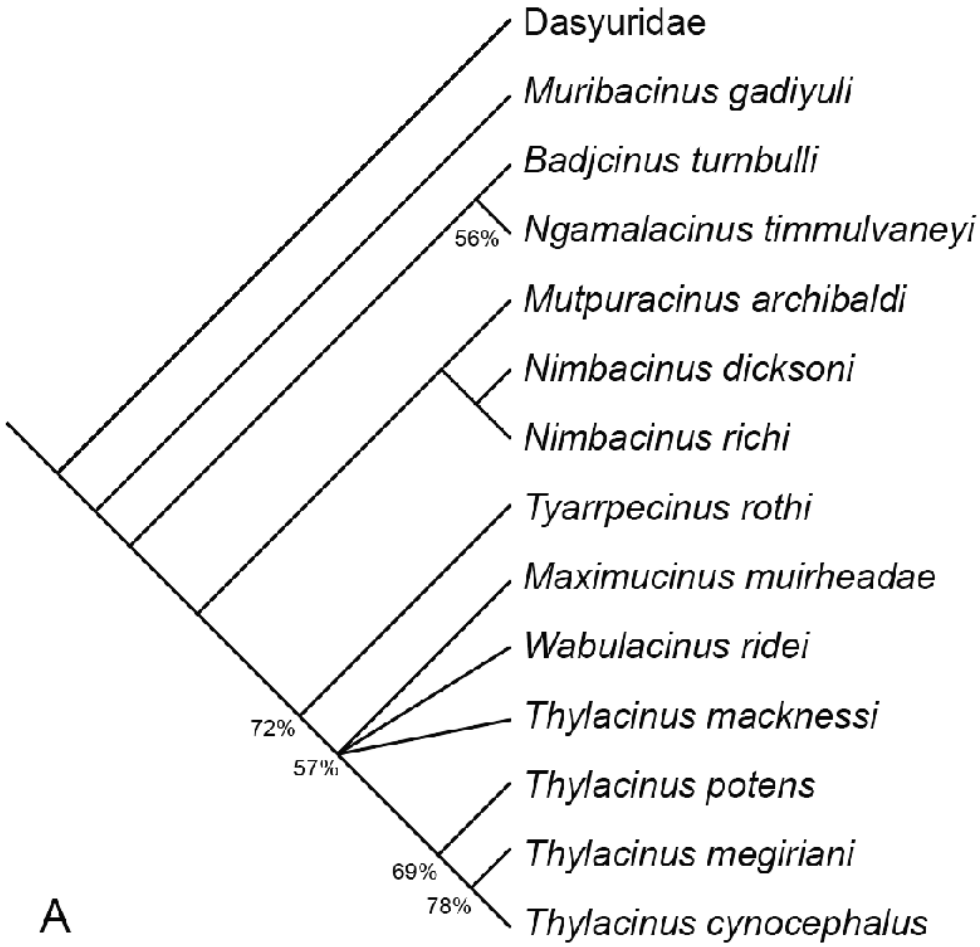

A

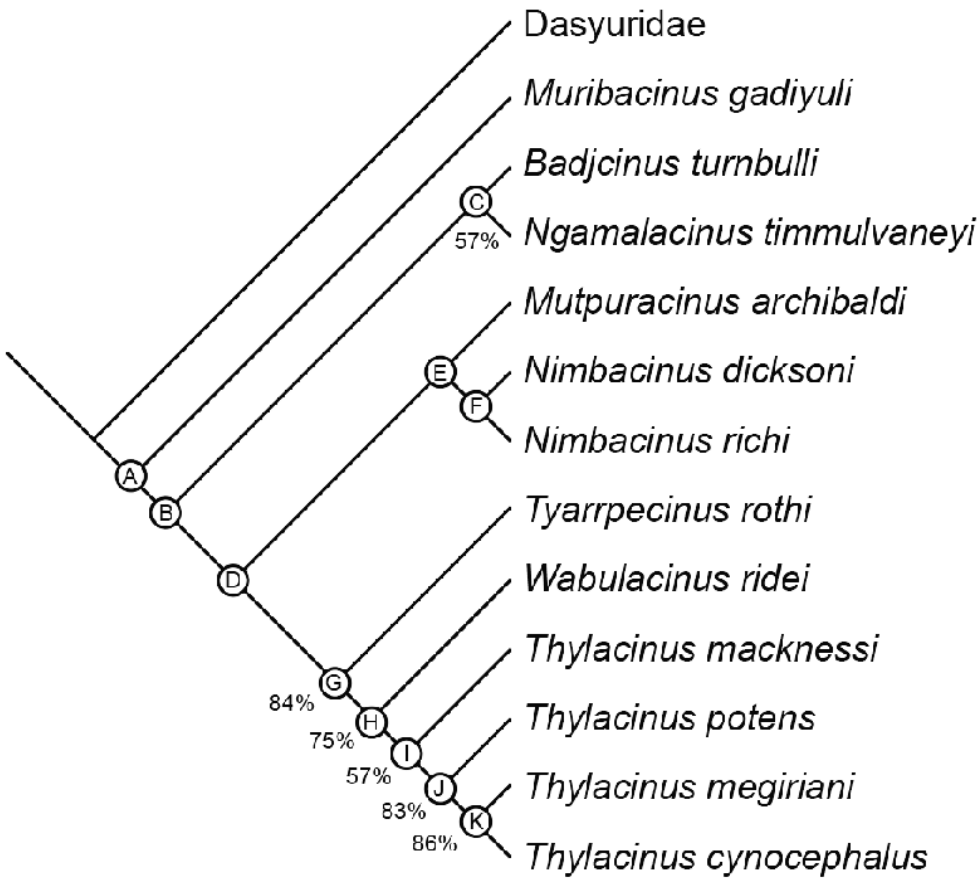

B

Table 1(on next page)

Terminal taxa

Table 1. Terminal taxa used in the cladistic analysis and their sources of character data (literature and specimens).

Taxon	Sources
Dasyuridae	Wroe, 1999 (*Barinya wangala*); NTM U7542 (*Dasyurus maculatus*)
Muribacinus gadiyuli	Wroe, 1996
Badjcinus turnbulli	Muirhead & Wroe, 1998
Ngamalacinus timmulvaneyi	Muirhead, 1997
Maximucinus muirheadae	Wroe, 2001
Mutpuracinus archibaldi	Murray & Megirian, 2000, 2006; NTM P907-3; NTM P9612-5
Nimbacinus dicksoni	Muirhead & Archer, 1990; Wroe & Musser, 2001
Nimbacinus richi	Murray & Megirian, 2000; NTM P9612-4; NTM P9973-11
Wabulacinus ridei	Muirhead, 1997
Tyarrpecinus rothi	Murray & Megirian, 2000; NTM P98211
Thylacinus macknessi	Muirhead, 1992; Muirhead & Gillespie, 1995
Thylacinus potens	Woodburne, 1967; CPC 6746(c); NTM P4326; NTM P4327
Thylacinus megiriani	Murray, 1997; NTM P4376; NTM P4377; NTM P9618
Thylacinus cynocephalus	Murray & Megirian, 2006; SAM M95, SAM M665/001, SAM M922, SAM M1952-56, SAM M1959-60.

Table 2(on next page)

Cranial measurements and ratio for *Thylacinus* species.

Table 2. Selected cranial measurements and ratio of *Thylacinus potens* and *Th. cynocephalaus*. MH, vertical height of the maxilla above the mesial end of P^3; C-P^3, the distance between the mesial margin of the upper canine and the distal margin of P^3; MH/C-P^3, ratio of maxilla height to canine-P^3distance; P^1-P^1, transverse distance between the left and right lingual sides of the distal roots of each P^1; DD, depth of the horizontal ramus of the dentary measured at the level of the mesial end of M_4. Measurements in mm, ~ indicates an approximation due to damage, * indicates a transverse measurement obtained by doubling the distance from the landmark to the midline. Measurements for *Th. cynocephalus* were obtained from a sample of nine adult specimens held at SAM.

	MH	C-P^3	MH/C-P^3	P^1-P^1	DD
Th. potens					
NTM P4326	44.4	~66.0	67.3%	19.2*	
NTM P4327					30.3
UCMP 66206					37.0
Th. cynocephalus					
mean	34.6	52.2	66.2%	22.1	27.2
range	28.8 - 40.7	45.8 - 58.52	63.9 % -70.5 %	18.9 - 23.9	22.1 - 31.0

Table 3(on next page)

Measurements of upper premolars

Table 3. Measurements of upper premolars of *Thylacinus potens* and *Th. cynocephalus*. Data for CPC 6746 and *Th. cynocephalus* are taken from Woodburne (1967). Measurements for *Th. cynocephalus* are mean values taken from a sample of six specimens. Measurements are in mm, ~ indicates an approximation due to damage. L = mesiodistal length, W = maximum buccolingual width.

	P^1L	P^1W	P^2L	P^2W	P^3L	P^3W
Th. potens						
NTM P4326	~13.3	4.8	14.2	6.7	15.8	8.7
NTM P4332	-	-	-	-	16.7	9.4
CPC 6746	-	-	12.4	5.5	16.0	8.8
Th. cynocephalus						
mean	6.2	3.3	8.3	3.8	10.6	5.0

Table 4(on next page)

Measurements of upper molars

Table 4. Measurements of upper molars of *Thylacinus potens* and *Th. cynocephalus*. Data for CPC 6746 and *Th. cynocephalus* are taken from Woodburne (1967). Measurements for *Th. cynocephalus* are mean values taken from a sample of six specimens. Measurements are in mm. L = mesiodistal length, W1 = width of the crown from the mesiobuccal corner to the lingual side of the protocone, W2 = width of the crown from the metastylar corner to the lingual side of the protocone.

	M^1W1	M^2L	M^2W1	M^2W2	M^3L	M^3W1	M^3W2	M^4L	M^4W1	M^4W2
Th. potens										
NTM P4326	12.4	15.7	14.7	18.0	16.0	15.5	18.6	11.5	14.0	9.5
NTM P4379	-	16.1	~14.1	~17.7	-	-	-	-	-	-
CPC 6746	12.8	15.7	13.9	17.5	15.2	15.9	19.0	12.2	15.8	9.9
Th. cynocephalus										
mean	7.8	13.2	10.0	15.0	15.1	12.0	17.8	9.7	12.6	7.8

Table 5(on next page)

Measurements of lower premolars

Table 5. Measurements of lower premolars of *Thylacinus potens* and *Th. cynocephalus*. Measurements for *Th. cynocephalus* are mean values taken from a sample of six specimens. Measurements are in mm. L = mesiodistal length, W= maximum buccolingual width.

	P_1W	P_1L	P_2W	P_2L	P_3W	P_3L
Th. potens						
NTM P4327	~4.9	12.7	5.6	15.5	6.8	14.8
Th. cynocephalus						
mean	3.4	6.0	4.1	9.1	5.0	10.6

Table 6(on next page)

Measurements of lower molars

Table 6. Measurements of lower molars of *Thylacinus potens* and *Th. cynocephalus*. Data for UCMP 66206 are taken from Woodburne (1967). Data for *Th. cynocephalus* are mean values taken from Woodburne (1967) and Dawson (1982). Measurements are in mm. L = mesiodistal length, W1 = width of the trigonid, W2 = width of the talonid.

	M_1L	M_1W1	M_1W2	M_2L	M_2W1	M_2W2	M_3L	M_3W1	M_3W2	M_4L	M_4W1	M_4W2
Th. potens												
NTM P4326	14.8	6.7	7.9	16.3	(7.3)	8.5	15.3	8.6	8.5	17.7	9.9	6.5
UCMP 66206	-	-	-	13	6.8	6.8	14.5	8.3	6.2	15.4	8.8	5.1
Th. cynocephalus												
Mean (Woodburne)				12.0	5.7	6.2	14.0	6.9	6.8	16.0	7.8	4.3
Mean (Dawson)	9.6	4.4		12.0	5.7		14.1	6.9		15.7	7.6	

Table 7(on next page)

Mass estimates for the new specimens of *Thylacinus potens.*

Table 7. Mass estimates for two of the new specimens of *Thylacinus potens*. Regression equations derived by Myers (2001) from his dasyuromorphian dataset. Abbreviations: 2UMW, width of the second upper molar; UMRL, upper molar row length; LMRL, lower molar row length.

Specimen	Method	Regression Equation	Measurement (mm)	Smearing Estimate (%)	Mass Estimate (kg)	Percentage Error Estimation (%)
NTM P4326	Regression of 2UMW	log y = 0.379 + 4.038(log x)	14.7	3	120.6	21
	Regression of estimated UMRL	log y = –0.992 + 3.279(log x)	51	1.2	40.9	14
	Geometric Similitude		43.2		43.3	
NTM P4327	Regression of LMRL	log y = –1.075 + 3.209(log x)	63.3	3	56.1	13
	Geometric Similitude		63.3		56.0	